A New Efficient Multiple Constraint Approach for Finite Element Analysis of Radius-cut RBS Moment Frames

By

Dawit Hailu

A Thesis Submitted to the Graduate School of the Addis Ababa University in Partial Fulfillment of the Requirements for the Degree of Master of Science in Civil Engineering

Addis Ababa

February 2004

ADDIS ABABA UNIVERSITY
SCHOOL OF GRADUATE STUDIES
FACULTY OF TECHNOLOGY
DEPARTMENT OF CIVIL ENGINEERING

A New Efficient Multiple Constraint Approach for Finite Element Analysis of Radius-cut RBS Moment Frames

Dawit Hailu

February 2004

Approved by Board of Examiners

Dr. -Ing Adil Zekaria Advisor	Signature	Date
External Examiner	Signature	Date
Internal Examiner	Signature	Date
Chairman	Signature	Date

Acknowledgements

Many thanks to my internal supervisor Dr.-Ing Adil Zekaria who was always there whenever I needed help. His continuous and timely help has made the successful completion of the work possible. His support on technical as well as non-technical matters is greatly appreciated. Moreover, his very friendly approach has made things much easier for me in the course of the work.

My deep gratitude also goes to my external supervisor Dr. Samuel Kinde of the University of California, Irvine. He was very helpful right from the beginning and provided possible research topics including the one undertaken in this work. His help was very thorough and timely at any stage of the work. Besides the practical help, he was a source of inspiration throughout the work.

I extend my thanks to Dr. Dermot Monaghan at the Queen's University of Belfast, Ireland for being kind enough to provide the full document of his Ph.D. thesis on request and for his useful comments on my work.

I would like to thank my family, especially my mother for her constant support. I would also like to thank my dear friend Daniel Teklu for his moral and practical help during the work. Without his help completion of the work would have been literally impossible. I also wish to thank my friends Tezera Firew, Riyad Ahmed, Samson Takele, Surafel Fekadu, Daniel Abera and Assegidew Dagne for their encouragement and understanding.

Table of Contents

List of Figures

List of Figures (contd.)

List of Tables

List of Appendices

List of Symbols

a , b , c	RBS geometric parameters
R	Radius of RBS cut
h	Beam depth
b_f	Flange width
t_w	Web thickness
$\lfloor \varepsilon_x \quad \varepsilon_y \quad \varepsilon_z \quad \gamma_{xy} \quad \gamma_{yz} \quad \gamma_{zx} \rfloor$	Normal and shear strains
$\lfloor \sigma_x \quad \sigma_y \quad \sigma_z \quad \tau_{xy} \quad \tau_{yz} \quad \tau_{zx} \rfloor$	Normal and shear stresses
E	Young's modulus
ν	Poisson ratio
G	Shear modulus
Φ_x, Φ_y, Φ_z	Surface tractions in the x, y and z directions
Π_p	Potential energy
$[N]$	Shape function matrix
$[k], [K]$	Element and global stiffness matrices
$\{r_e\}$, $\{R\}$	Element and global load vector
$\{d\}$, $\{D\}$	Element and global nodal displacements
ξ , η , ζ	Natural coordinates
λ_i	Lagrange multipliers
α_i	Penalty numbers
F_z	Axial force
F_y , F_x	Shear forces in the y and x directions
M_x , M_y	Bending moments about the x and y axes
M_z	Torsional moment
$\lfloor u \quad v \quad w \rfloor$	Beam node displacements in the x, y and z directions
$\lfloor U \quad V \quad W \rfloor$	Shell node displacements in the x, y and z directions
$\lfloor \theta_x \quad \theta_y \quad \theta_z \rfloor$	Beam and shell node rotations about x, y and z axes

Abstract

Following the 1994 Northridge, California Earthquake engineers realized that the traditional beam-column connection in moment frames was in fact brittle and thus unsafe. Extensive research was subsequently undertaken resulting in improved and safe connection details. Among the new and pre-qualified connection details is the Reduced Beam Section (RBS) moment connection. In RBS moment connections a portion of the beam flange is removed near the connection thereby reducing the stress and strain demands in the connection.

Currently there is no accurate efficient and practical method for the analysis of moment frames with RBS connection. In this study, an accurate and efficient method for the linear elastic analysis of moment frames with RBS connection has been developed. The method is based on mixed dimensional finite element analysis. The connection region including some portion of the beam and column is modeled with shell elements, and the remaining part is modeled with computationally cheaper beam elements. Valid beam-shell transition is achieved using multi-point constraint equations derived by equating work on either side of the mixed dimensional interface. Normal and shear stress distributions at the interface have been assumed in accordance with simple beam theory. The derived constraint equations have been applied to specific examples using the general purpose finite element analysis program ANSYS. It has been found that the mixed models based on the derived constraint equations provide acceptably accurate and efficient analysis methods for moment frames with RBS connection.

Chapter 1
Introduction

Structural analysis (i.e., calculation of responses such as stresses and displacements as a result of applied loading) is one of the major components of the structural design process. The quality of the final design depends directly on the quality of the analysis method employed. Thus engineers have always strived for accurate analysis methods which provide realistic predictions of structural response. However, an accurate analysis method is usually achieved at the expense of increased computational time and effort. This requires that designers find an optimum point that balances the required accuracy and the corresponding computational cost.

Frame models (trusses, beams and frames) have in many cases proved to be very efficient and accurate analysis tools available to the engineer. While the use of frame models is in many ways advantageous, there are a number of factors which render the results of such analysis models inaccurate. One such factor is connection modeling. In typical frame models, the joint between individual members is assumed to be rigid, i.e., initial angles between members do not change, regardless of the particular connection detail. In addition results of frame models deviate significantly from the actual conditions near the joints due to stress concentrations although results away from the joints are justified by the application of the Saint Venant principle.

Connection performance has a profound effect on the overall safety of framed structures since connection failure will result in total collapse of framed structures. Thus connection performance should be studied to ensure sufficient strength, stiffness and ductility. Connection behavior can be studied using either empirical methods or numerical modeling techniques such as the finite element technique. Experimental testing of connections is most reliable and accurate but is expensive and time taking. The finite element technique provides a sufficiently accurate and less expensive method to study connection behavior.

The Reduced Beam Section (RBS) moment connection is a new and innovative technique in seismic design of moment frames whereby a portion of the beam flange is removed near joints in an effort to reduce stress at joints. The adoption of RBS connection is a result of extensive research undertaken in the US after the 1994 Northridge, California earthquake which exposed the fact that the conventional, pre-Northridge connection was actually not as ductile as believed to be. The basic idea behind the RBS connection is that by reducing the beam section near the joints, the stress and strain demands at the connection are decreased. It can be thought as a "fuse" that limits the stresses that can be transmitted to the connection. Moment frames with RBS connection are therefore expected to behave in ductile manner under severe loads by forming plastic hinges within the beam without connection failure.

Structural analysis should be in a position to accommodate new and innovative designs such as moment frames with RBS connection. The use of the conventional prismatic frame models to the analysis of moment frames with RBS connection is inappropriate since the effect of the RBS on stresses and displacements is too large to be neglected. In addition the localized nature of the RBS connection (especially the radius cut RBS) makes it inconvenient to be modeled as a series of non-prismatic beams. The frame model also has the general limitations mentioned above regarding connection models and stress concentration.

Current provisions such as FEMA* 350 [4] attempt to account for the effect of the RBS by simply increasing the drift by a certain percentage corresponding to the amount of flange reduction. Such methods are empirical in nature and are not based on sound principles of mechanics. In fact they are reported to underestimate the drift in some cases [7]. Thus there is a need for a more accurate but efficient analysis method for moment frames with RBS connection.

In this study an efficient and accurate method based on the finite element method for the linear static analysis of moment frames with RBS moment connection will be presented. The proposed method attempts to accurately model moment frames with RBS connection with a slightly higher computational effort than conventional frame model. The method is based on mixed dimensional finite element modeling of the moment frames with RBS connection. The joint region including the RBS connection is modeled by shell elements while the frame region away from the joints is modeled by beam elements. Thus the mixed model accurately predicts the stresses at RBS connection region. Coupling between the beam and shell elements is achieved via constraint equations which are derived so as to satisfy stress distributions in accordance to the theory of elasticity.

The contents of this presentation are organized as follows. In Chapter 2 background information on RBS connection is given. Here the origin of the RBS connection and the state of art on the analysis and design of moment frames with RBS connection is discussed. In Chapter 3, a brief revision of the basic ideas of linear elasticity, the finite element, and constraint equations is presented. Chapter 4 deals with coupling beam and shell elements in general. In Chapter 5, the application of the general beam-shell coupling technique to moment frames with RBS connection is illustrated. In Chapter 6, the validity of the developed coupling technique will be demonstrated using examples. Finally, in Chapter 7, conclusions are made based on the work undertaken, and directions for further work are indicated.

Chapter 2
Reduced Beam Section Connections

2.1 NORTHRIDGE EARTHQUAKE

Engineers have always considered steel moment-frame design to be appropriate solutions in seismic regions because of their perceived ductility. That myth was challenged after Jan. 17, 1994, when a 6.7-magnitude earthquake hit Northridge, California, and shook the Los Angeles Basin for 14 seconds [1]. The "pre-Northridge" (Fig. 2-1) moment connection was in fact brittle and thus more susceptible to collapse than previously believed. This connection (typically consisting of a bolted-beam web and full penetration welds from beam flanges to the column flange) needed to be modified. Subsequent examination revealed that a number of steel moment frames suffered severe damages. The California Seismic Safety Commission expressed concerns about the brittleness of the pre-Northridge connection and requested that the International Conference of Building Officials (ICBO) proclaim an emergency withdrawal of the building code provisions for the pre-qualified, pre-Northridge connection. The request was put to effect on Sept. 1994.

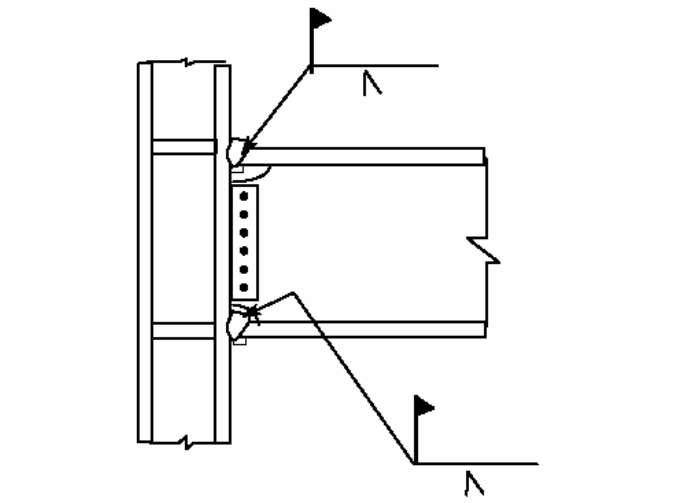

Fig. 2-1 Pre-Northridge Connection

What became known as the "pre-Northridge" connection was eventually dubbed "fundamentally flawed". Even though no moment frame building collapsed in the Northridge earthquake, the severity of the extent of the damages was alarming. An Earthquake which hit Kobe, Japan on Jan. 17, 1995, the exact day of the first anniversary of the Northridge earthquake proved to be much more fatal. More than 5,000 people were killed and, 35,000 people injured, and 30,000 more rendered homeless. A number of steel moment frame buildings experienced significant damage, confirming once more again that the myth that "steel moment frames are ductile" was not after all true for the pre-Northridge connection. Fig. 2-2 shows the common zone of crack initiation of the pre-Northridge connection during the Northridge earthquake.

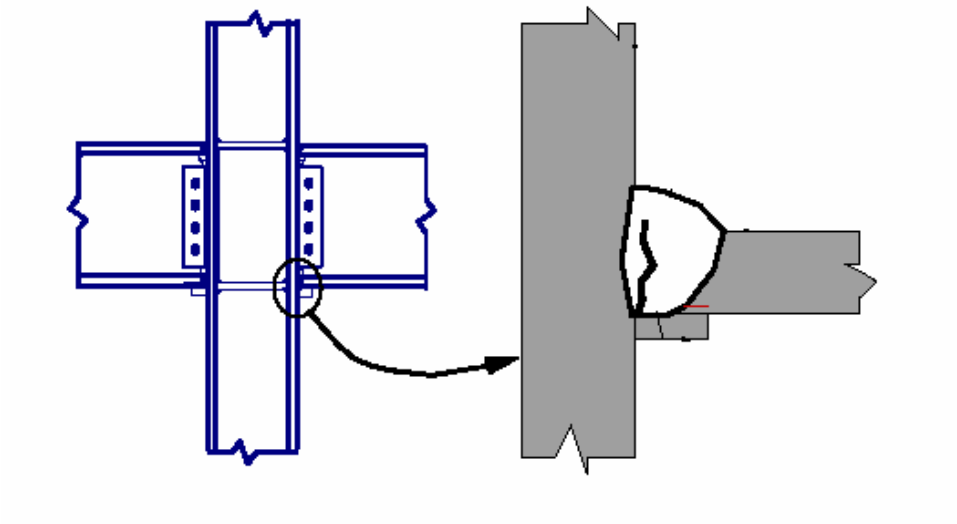

Fig. 2-2 Common Zone of Fracture Initiation [3]

The SAC joint venture came into existence with purpose of identifying the cause of the poor performance of steel moment frames and providing short and long term solutions. SAC is an acronym for the three participating organizations namely the Structural Engineers Association of California, Applied Technology Council, and the Consortium of Universities for Research in Earthquake Engineering SAC's main challenge was to research and design a new connection between steel columns and beams that could better withstand future earthquakes.

The SAC joint venture's task was done in two phases. Phase 1, which was initiated in late 1994 only lasted six months. It was intended to focus principally on investigation and repair of damaged buildings, with lesser emphasis on recommendations for designing new buildings and upgrading existing buildings. The goal of this phase was to develop interim solutions rapidly. Phase 2 of the project was more measured and ultimately extended over a five year period. The goal of this phase was to find the cause the cause of the adverse behavior first and then to find solutions.

After extensive research which consisted of testing and finite element modeling, it was found out that the poor performance of the standard connection was a result of a number of complex and inter-related factors. The main reasons identified were:

1. The geometry induced severe stress concentration in regions where material yielding was inhibited by triaxial restraint and where strength and toughness were highly sensitive to workmanship.
2. The geometry also made it difficult to weld without large defects that could lead to fractures and to inspect the welded joints reliably.
3. The increase in steel section sizes and changes in steel production processes made previous provisions no more applicable.

After Northridge earthquake, the designer of new steel moment frames had two options. In the first option, the designer is required to verify the adequacy of the connection design by full scale testing. A set of qualifying criteria were provided based on which the performance of the connections were evaluated. This option was clearly more expensive and discouraging engineers to use moment frames in new designs. In view of these, SAC provided an alternative option. The second option does not require the designer to undertake full scale connection design, but to choose one from a number of pre-qualified connection details. However, the designer is strictly required to use the pre-qualified connection details under conditions very similar to the tests and analyses which were used to qualify the connection. In other words, only limited extrapolation from the conditions of testing is allowed. The Reduced Beam Section moment connection is one of the pre-qualified connection details.

2.2 REDUCED BEAM SECTION (RBS) CONNECTIONS

Many of the new moment connections combine improvements in welding with some type of reinforcement at the connection (cover plates, ribs, haunches, side plate, etc.) [5]. The purpose of the reinforcement, in the most general terms, is to provide a connection that is stronger than the beam. A strong earthquake would be expected to develop plastic hinges at the beam ends in a traditional fully restrained moment frame. The reinforcement is intended to force the plastic hinge away from the face of the column, where premature fractures can occur due to potential weld defects, stress concentrations due to column flange bending, high levels of restraint and associated states of triaxial tension, etc. The reinforcement reduces stress levels within this vulnerable region near the column face, and forces large stresses and inelastic strains farther from the connection.

Reinforcing the connection, however, increases its cost. Further, if excessive reinforcement is used new problems can be created resulting from the need for very large welds with higher shrinkage, and higher degrees of restraint and triaxial tension. An alternative to reinforcing a moment connection that provides benefits similar to reinforcement, but may avoid some of the disadvantages, is the "dogbone" moment connection. A distinguishing feature of the dogbone, also known as the Reduced Beam Section (RBS) connection, is that portions of the beam flange are trimmed away in the region adjacent to the beam-to-column connection. Various shape cutouts are possible. The result is similar to reinforcement, i.e., the connection is stronger than the beam. In this case, however, the connection is made stronger than the beam not by increasing the strength of the connection, but rather by decreasing the strength of the beam. The dogbone can be viewed as a ductile fuse. It forces yielding to occur within the reduced section of the beam, an area that can sustain large inelastic strains. At the same time, the dogbone acts as a fuse, limiting stress at the less ductile region near the face of the column.

The basic concept of reduced beam section is the reduction of a beam flange near the beam-column connection, and the actual geometry of the cut may be of various types . The common types of the RBS geometries are the constant cut, tapered cut or the radius cut (Fig. 2-3).

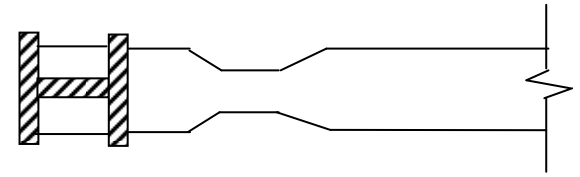

(a) Constant cut RBS

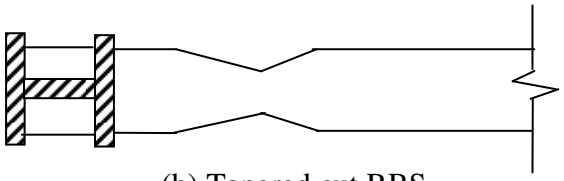

(b) Tapered cut RBS

(c) Radius cut RBS

Fig. 2-3 Types of RBS Connections

Research on RBS indicates that they can go a long way toward eliminating or at least substantially reducing earthquake induced cracking at welded moment connections [6]. Research conducted have demonstrated the superiority of the radius (or curved) cut. With the angular cuts cracks would tend to develop when the beams were subjected to high forces. Testing of radius cut at the University of Texas at Austin indicates the enhanced safety of the beam.

It was reported that a testing rotation of 0.1 radians, or about 1% rotation (which was the estimated force of the Northridge earthquake), there was a slight demand on the ductility of the beam. Increasing the rotation to 0.2 radians still resulted in some minor yielding.

At 0.4 radians - from three to four times the Northridge - some local beam buckling was finally observed. But the beam was still connected to the column and it is holding the load. But it was recommended that one should never remove more than 50% of the total beam flange be removed.

Welds of beam flanges to column in RBS connections are complete joint penetration groove welds, meeting the requirements of FEMA 350 [4]. In this type of connection, no reinforcement, other than the weld metal, is used to join the flanges of the beam to the column. Web welds for this type of connection may either be complete penetration groove welds, or bolted or welded shear tabs. Fig. 2-4 provides typical details for this connection type.

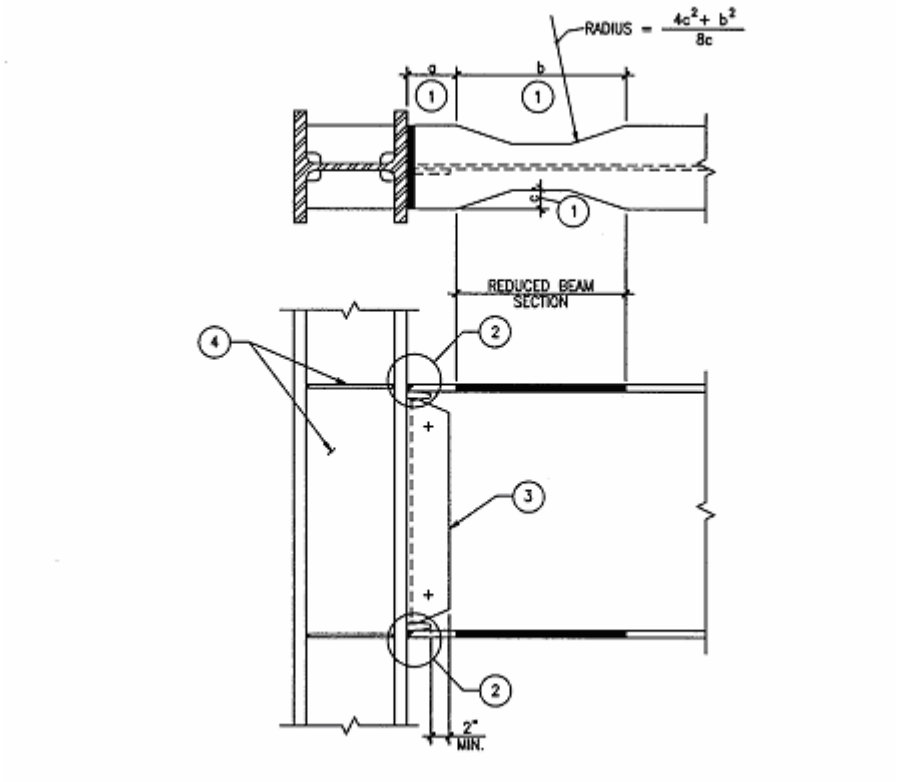

Fig. 2-4 Reduced Beam Section Connection Detail [4]

The design procedure for RBS connections has been outlined in FEMA 350 [4]. The following recommendations for the dimensions of reduced beam section parameters are given:

$$\begin{aligned} a &\cong (0.5 \text{ to } 0.75) b_f \\ b &\cong (0.65 \text{ to } 0.85) h \\ c &\cong (0.20 \text{ to } 0.25) b_f \end{aligned} \quad \text{... (2-1)}$$

where a, b and c are geometric parameters of the RBS shown in Fig. 2-5, b_f is the flange width, and h is the beam depth.

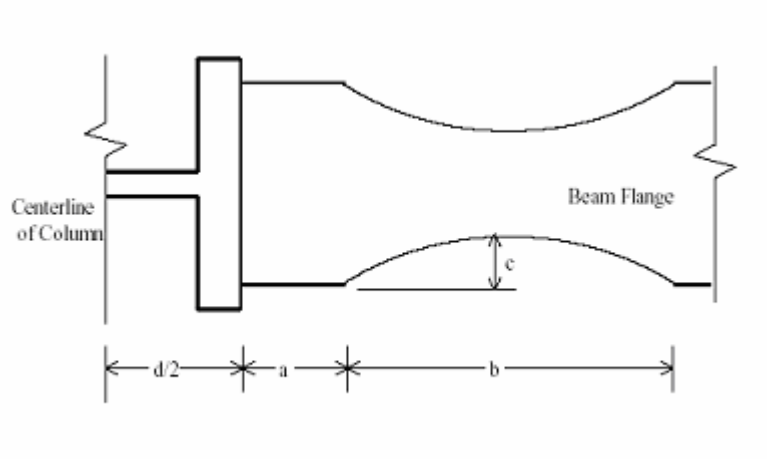

Fig. 2-5 RBS Geometric Parameters

From simple geometry the radius of the cut R is given by:

$$R = \frac{4c^2 + b^2}{8c} \quad \text{...(2-2)}$$

2.3 CURRENT ANALYSIS OF MOMENT FRAMES WITH RBS CONNECTIONS

It is clear that the presence of RBS will affect the structural response (stresses and displacements) of moment frames with RBS connections, and this has to be taken into account in the design process. Current design practice takes into account the effect of RBS by increasing the elastic drift by 9% corresponding for flange reduction of 50% of the beam flange width, with linear interpolation for lesser values of beam flange reduction [4]. This approach is simple to use but is not based on sound principles of mechanics. In addition, the results of this approach do not necessarily give conservative results. In fact it has been shown that in some cases that the actual drift obtained by a more exact analysis to be much larger than that predicted by the above simple rule [7]. Moreover, the above rule does not provide any information as to the effect of the RBS on the stress distribution, especially at and near the connection. Therefore, there is a need for a more accurate and at the same time efficient analysis method for moment frames with RBS connections.

The aim of this study is to present a new efficient approach for the analysis of moment frames with RBS which is based on mixed dimensional finite element modeling. The study will be limited to linear static analysis of special moment frames with RBS connections.

Chapter 3
Review of Basic Concepts

3.1 INTRODUCTION

A brief discussion of basic concepts of linear elasticity, the finite element method and constraint equations will be presented. Before dealing with the main topic of the study (i.e., analysis of moment frames with RBS connection) a review of some established yet relevant concepts of structural mechanics will be helpful in providing the necessary ground work for subsequent discussion. The discussion of linear elasticity is important since the main objective of the thesis work is linear elastic analysis of moment frames with RBS connection. Theory of elasticity, even though inapplicable in most practical cases, provides conditions that must be satisfied for an exact solution of a linear elastic analysis, and thus provides a measure of accuracy for problems solved using other methods. The finite element method deserves special treatment since the proposed method for the analysis of moment frames with RBS connection is based on the finite element method. Special discussion of constraint equations has also be given as it is a core idea in the suggested mixed dimensional finite element formulation for the analysis of moment frames with RBS connection.

3.2 LINEAR ELASTICITY

The main goal of both classical mechanics of materials and theory of elasticity is stress analysis, i.e., finding stress and displacement field of a body subjected to prescribed loading and boundary conditions. However, there is a fundamental distinction on how mechanics of materials and theory of elasticity attempt to solve a problem.

Analysis based on mechanics of materials typically depends on certain valid assumptions on the geometry of deformation which are then supplemented by material stress-deformation behavior and equilibrium to arrive at the solution. In theory of elasticity stress analysis is fundamentally reduced to solving certain governing partial differential equations.

A brief discussion of the basic ideals of the theory of elasticity will follow. Theory of elasticity is a highly mathematical method of solving stress analysis problems. It is based on three basic concepts: stress-strain relationship, equilibrium and boundary conditions.

3.2.1 Stress and Strain

Stress and strain are basic in structural mechanics. Stress is a measure of intensity of force on which material response is highly dependent. Strain is a measure of deformation, and is related to displacement field by the strain-displacement relationships. For infinitesimal deformation strain-displacement relations take the following form:

$$\varepsilon_x = \frac{\partial u}{\partial x} \qquad \varepsilon_y = \frac{\partial v}{\partial y} \qquad \varepsilon_z = \frac{\partial w}{\partial z} \qquad \text{... (3-1a)}$$

$$\gamma_{xy} = \frac{\partial u}{\partial y} + \frac{\partial v}{\partial x} \qquad \gamma_{xz} = \frac{\partial u}{\partial z} + \frac{\partial w}{\partial x} \qquad \gamma_{yz} = \frac{\partial v}{\partial z} + \frac{\partial w}{\partial y} \qquad \text{... (3-1b)}$$

where $\lfloor u \quad v \quad w \rfloor$ is the displacement field in the *x*, *y* and *z* directions, respectively, and $\lfloor \varepsilon_x \quad \varepsilon_y \quad \varepsilon_z \quad \gamma_{xy} \quad \gamma_{yz} \quad \gamma_{zx} \rfloor$ is the strain filed.

For a given material there exists a specific empirical relation between the applied stress and the corresponding strain. Generally, ignoring thermal effects, the stress-strain relationship for a particular material can be written in the form:

$$\{\varepsilon\} = [C]\{\sigma\} \qquad \text{or} \qquad \{\sigma\} = [E]\{\varepsilon\} \qquad \text{... (3-2)}$$

where

$\{\sigma\}^T = \lfloor \sigma_x \quad \sigma_y \quad \sigma_z \quad \tau_{xy} \quad \tau_{yz} \quad \tau_{zx} \rfloor^T$ is the applied stress,

$\{\varepsilon\}^T = \lfloor \varepsilon_x \quad \varepsilon_y \quad \varepsilon_z \quad \gamma_{xy} \quad \gamma_{yz} \quad \gamma_{zx} \rfloor$ is the corresponding strain.

$[C]$ is a symmetric matrix of *material compliances*, $[E]$ is a symmetric matrix of *material stiffnesses*, and $[E] = [C]^{-1}$. Eq. 3-2 is the most general form of Hooke's law. In the most general case of *anisotropy* $[C]$ and $[E]$ each contain 21 independent coefficients. O*rthotropic* material exhibit extreme values of stiffness in mutually perpendicular directions and nine parameters are needed to completely specify material behavior. In the most ideal case of *isotropy* the material behavior is independent of direction. In such case only two quantities (typically the Young's modulus E and the Poisson ratio ν) are needed to define the stress-strain relation. Hooke's law the case of isotropy can be written as:

$$\begin{aligned} \varepsilon_x &= \frac{1}{E}\left[\sigma_x - \nu(\sigma_y + \sigma_z)\right] \\ \varepsilon_y &= \frac{1}{E}\left[\sigma_y - \nu(\sigma_x + \sigma_z)\right] \\ \varepsilon_x &= \frac{1}{E}\left[\sigma_z - \nu(\sigma_x + \sigma_y)\right] \end{aligned} \qquad \text{... (3-3a)}$$

$$\begin{aligned} \gamma_{xy} &= \tau_{xy}/G \\ \gamma_{yz} &= \tau_{yz}/G \\ \gamma_{zx} &= \tau_{zx}/G \end{aligned} \qquad \text{... (3-3b)}$$

where G is the shear modulus, and given by $G = E/2(1+\upsilon)$.

3.2.2 Equilibrium

By considering an infinitesimal element of a body in equilibrium, differential equations of equilibrium may be derived. In Cartesian systems, the equations of equilibrium in three dimensions may be written as:

$$\frac{\partial \sigma_x}{\partial x} + \frac{\partial \tau_{xy}}{\partial y} + \frac{\partial \tau_{xz}}{\partial z} + F_x = 0$$
$$\frac{\partial \tau_{xy}}{\partial x} + \frac{\partial \sigma_y}{\partial y} + \frac{\partial \tau_{yz}}{\partial z} + F_y = 0 \qquad \text{... (3-4)}$$
$$\frac{\partial \tau_{xz}}{\partial x} + \frac{\partial \tau_{yz}}{\partial y} + \frac{\partial \sigma_z}{\partial z} + F_z = 0$$

where F_x, F_y and F_z are body forces per unit volume in the *x*, *y* and *z* directions, respectively. The above equations should be satisfied at each and every point within a body.

3.2.3 Boundary Conditions

The equations of equilibrium must be satisfied not only within a body but also on the boundary of the body. The stress distribution on the boundary must be in equilibrium with the external forces on the surface of the body. These boundary conditions of equilibrium may be written as:

$$\Phi_x = l\sigma_x + m\tau_{xy} + n\tau_{zx}$$
$$\Phi_y = l\tau_{xy} + m\sigma_y + n\tau_{yz} \qquad \text{... (3-5)}$$
$$\Phi_z = l\tau_{zx} + m\tau_{yz} + n\sigma_z$$

where l, m, and n are the direction cosines of the outward normal to the surface

Φ_x, Φ_y and Φ_z are the surface tractions in the *x*, *y* and *z* directions.

3.2.4 Compatibility

The six components of strain at any given point are completely determined by three functions u, v and w representing the components of displacement. It is necessary to consider the elastic deformations of the material such that, in a continuous strain field, the displacements are compatible with the stress distribution.

Therefore, the components of the strain cannot be taken arbitrarily as functions of *x*, *y* and *z,* but are subject to relations.

If there are no body forces, or if the body forces are constant, the relations are as follows:

$$
\begin{aligned}
&(1+\nu)\nabla^2\sigma_x + \frac{\partial^2\lambda}{\partial x^2} = 0 \qquad && (1+\nu)\nabla^2\tau_{yz} + \frac{\partial^2\lambda}{\partial y\partial z} = 0 \\
&(1+\nu)\nabla^2\sigma_y + \frac{\partial^2\lambda}{\partial y^2} = 0 \qquad && (1+\nu)\nabla^2\tau_{xz} + \frac{\partial^2\lambda}{\partial x\partial z} = 0 \\
&(1+\nu)\nabla^2\sigma_z + \frac{\partial^2\lambda}{\partial z^2} = 0 \qquad && (1+\nu)\nabla^2\tau_{xy} + \frac{\partial^2\lambda}{\partial x\partial y} = 0
\end{aligned}
\qquad \text{... (3-6)}
$$

where $\lambda = \sigma_x + \sigma_y + \sigma_z$ and $\nabla^2 = \frac{\partial^2}{\partial x^2} + \frac{\partial^2}{\partial y^2} + \frac{\partial^2}{\partial z^2}$

For a linearly elastic body if one finds a stress field or a displacement field that simultaneously satisfies equilibrium, compatibility, and boundary conditions, then one have found a solution to the problem posed. Moreover, the solution is both unique and exact within the assumptions made.

3.3 FINITE ELEMENT METHOD

Theory of elasticity, despite its elegance, is of limited practical use. Exact solutions based on the theory of elasticity are possible in very few cases which are too idealized to be of any practical value. Thus one resorts to numerical techniques to solve practical problems typically involving complex geometry, loading and boundary conditions. The finite element method is probably the most important numerical method for the solution of stress analysis as well as many other engineering problems. With increasing development in computing capability, the finite element method is finding widespread use in many areas of engineering. A brief discussion on the basics of the finite element in the context of structural mechanics method will follow. A special attention will be given to the topic constraint equations which is an important part of this study.

The finite element is enjoying an ever increasing application in the solution of real life engineering problems. The method was initially developed based on the physical concept of "stiffness". Now the method is recognized as a basic numerical technique for the solution certain type of partial differential equations.

The finite element method is in itself a very wide topic, and it is by no means possible to include a detailed discussion here. Only the very basic ideas of the finite element method which are relevant to this investigation will be briefly described.

The finite element may be formulated by considering either the displacements or the stresses or a combination of both as the basic variables. If the displacements are chosen as the prime unknowns, with the stresses being determined from the calculated displacement field, the process is termed the *displacement method* [8]. Alternatively, it is possible to proceed with the stresses as the prime unknowns, an approach which is termed the *force method*. If both stresses and displacements are employed as variables simultaneously the method is said to be *mixed* or *hybrid.* The displacement based finite element is the most widely employed approach and it is appealing to engineers because of its similarity to the displacement method of matrix structural analysis.

3.3.2 Basic Derivation of Displacement Based FEM

The basic procedures in the displacement based finite elements for structural mechanics can be summarized as follows [9]. Displacements are taken as the primary unknowns. Then an appropriate displacement field is defined in a piecewise fashion so that displacements within any element are interpolated from the nodal degrees of freedom (d.o.f.) of that element. Using the *principle of stationary potential energy*, we set the derivative of the total potential energy with respect to each nodal d.o.f. to zero, from which we obtain algebraic equations to be solved for nodal d.o.f. In the course of this argument we identify certain expressions we identify as the element stiffness matrix $[k]$ and the element load vector.

Details of the derivation are described below. The starting point is the expression for potential energy in a linearly elastic body:

$$\Pi_p = \int_V \left[\frac{1}{2} (\{\varepsilon\}^T [E] \{\varepsilon\} - \{\varepsilon\}^T [E] \{\varepsilon_0\} + \{\varepsilon\}^T \{\sigma_0\}) \right] dV - \int_V \{u\}^T \{F\} dV - \int_S \{u\}^T \{\Phi\} dS - \{D\}^T \{P\} \quad \text{... (3-7)}$$

in which $\{u\} = \lfloor u \quad v \quad w \rfloor^T$, the displacement field (in the x, y, and z directions respectively)

$\{\varepsilon\} = \lfloor \varepsilon_x \quad \varepsilon_y \quad \varepsilon_z \quad \gamma_{xy} \quad \gamma_{yz} \quad \gamma_{zx} \rfloor$, the strain field

$[E]$, the material property matrix

$\{\varepsilon_0\}, \{\sigma_0\}$, initial stress and strains

$\{F\} = \lfloor F_x \quad F_y \quad F_z \rfloor$, body forces

$\{\Phi\} = \lfloor \Phi_x \quad \Phi_y \quad \Phi_z \rfloor$, surface tractions

$\{D\}$, nodal d.o.f.

$\{P\}$ = nodal forces

S, V = surface area and volume

Displacements within an element are interpolated from element nodal d.o.f. $\{d\}$:

$$\{u\} = [N] \{d\} \quad \text{... (3-8)}$$

where $[N]$ is the *shape function matrix*.

Strains are obtained from displacements by differentiation:

$$\{\varepsilon\} = [\partial] \{u\} \quad \text{yields} \quad \{\varepsilon\} = [B] \{d\} \quad , \text{ where} \quad [B] = [\partial] [N] \quad \text{... (3-9)}$$

Substitution of the expression for $\{u\}$ and $\{\varepsilon\}$ into Eq.(3-7) yields:

$$\Pi_p = \frac{1}{2}\sum_{n=1}^{numel}\{d\}_n^T[k]_n\{d\}_n - \sum_{n=1}^{numel}\{d\}_n^T\{r_e\}_n - \{D\}^T\{P\} \quad \text{... (3-10)}$$

where summation symbols indicate that we include contributions from all elements of the structure, and we have defined:

Element stiffness matrix:

$$[k] = \int_{V_e}[B]^T[E][B]dV \quad \text{... (3-11)}$$

Element load vector:

$$\{r_e\} = \int_{V_e}[B]^T[E]\{\varepsilon_0\}dV - \int_{V_e}[B]^T\{\sigma_0\}dV + \int_{V_e}[N]^T\{F\}dV + \int_{S_e}[N]^T\{\Phi\}dS \quad \text{... (3-12)}$$

where V_e denotes the volume of an element and S_e its surface. In the surface integral, $[N]$ is evaluated on S_e.

Every d.o.f. in an element vector $\{d\}$ also appears in the vector of global (i.e., structural) d.o.f. $\{D\}$. Therefore $\{D\}$ can replace $\{d\}$ in Eq.(3-10) as follows:

$$\Pi_p = \frac{1}{2}\{D\}^T[K]\{D\} - \{D\}^T\{R\} \quad \text{... (3-13)}$$

where

$$[K] = \sum_{n=1}^{numel}[k]_n \quad \text{and} \quad \{R\} = \{P\} + \sum_{n=1}^{numel}\{r_e\}_n \quad \text{... (3-14)}$$

$[K]$ is the *global/ structure stiffness matrix*, and $\{R\}$ is the *global/ structure load vector*.

Using the *principle of stationary potential energy*, the derivatives of Π_p with respect to each d.o.f. D_i is set to zero:

$$\left\{\frac{\partial \Pi_p}{\partial D}\right\} = \{0\} \qquad \text{yields} \qquad [K]\{D\} = \{R\} \qquad \text{... (3-15)}$$

The latter of the equations in Eq.(3-15) is a set of simultaneous equations to be solved for d.o.f. $\{D\}$.

The steps in the displacement based finite element may be summarized as follows:

1. The structure is divided into a number of finite elements (meshing).
2. The stiffness of each element is calculated. Element stiffness is in some cases computed using explicit formulas (e.g. truss and frame elements). Stiffness of continua elements is usually found by integrating Eq. 3-11 numerically.
3. Element stiffness matrices are assembled to form the structure or global stiffness matrix (Eq. 3-14).
4. Force and displacement boundary conditions are imposed.
5. A set of simultaneous linear equations are solved to determine nodal d.o.f. which are displacements.
6. Strains and stresses are then computed from the known values of displacements.

The user of a commercial finite element package does not participate actively in all the above steps. The user may have some control in meshing, is required to specify the force and displacement boundary conditions, and finally to interpret the final output. The remaining steps (major part of the meshing, element stiffness computation, assembly, solution, stress calculation) are done internally by the program.

3.3.3 Isoparametric Formulation

The *isoparametric formulation* makes it possible to generate elements that are nonrectangular and have curved sides. In formulating isoparametric elements, natural coordinates $\xi\eta\zeta$ must be used. Displacements are expressed in terms of natural coordinates, but must be differentiated with respect to global coordinates *x*, *y*, and *z*. Therefore, a transformation matrix, called, the Jacobian matrix, must be used.
In addition integration must be done numerically rather than analytically if the elements are non-rectangular.

The term "isoparametric" means "same parameters" and in isoparametric formulation the same shape functions are used to interpolate coordinates and d.o.f. Suppose that the displacements $\lfloor u \quad v \quad w \rfloor$ and coordinates $\lfloor x \quad y \quad z \rfloor$ are interpolated using the shape functions $[N]$ and $[\tilde{N}]$, respectively. That is

$$\lfloor u \quad v \quad w \rfloor = [N]\{d\} \qquad \text{and} \qquad \lfloor x \quad y \quad z \rfloor = [\tilde{N}]\{c\} \qquad \text{... (3-16)}$$

where $\{d\}$ and $\{c\}$ are nodal displacements and nodal coordinates, respectively. Shape function matrices $[N]$ and $[\tilde{N}]$ are functions of the natural coordinate components ξ, η and ζ. An element is *isoparametric* if $[N]$ and $[\tilde{N}]$ are identical.

The concept of isoparametric finite element formulation will illustrated using a plane quadrilateral element (Fig. 3-1).

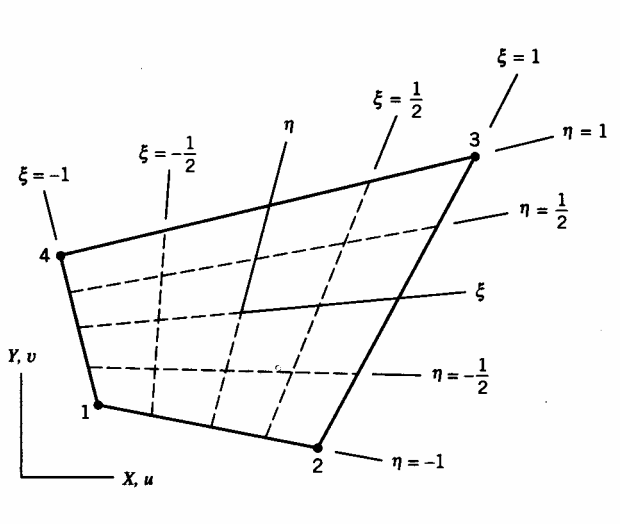

Fig. 3-1 Four Node Plane Isoparametric Element [10]

A natural coordinate system $\xi\eta$ is introduced. In the natural coordinate system the element sides are always defined by $\xi = \pm 1$ and $\eta = \pm 1$, regardless of the shape or physical size of the element or its orientation in the global coordinates XY. Coordinates of a point within the element are defined by:

$$X = \sum N_i X_i \qquad Y = \sum N_i Y_i \qquad \text{... (3-17)}$$

in which X_i and Y_i are the coordinates of the corner nodes and the shape (or interpolation) functions N_i are:

$$\begin{aligned} N_1 &= \frac{1}{4}(1-\xi)(1-\eta) & N_2 &= \frac{1}{4}(1+\xi)(1-\eta) \\ N_3 &= \frac{1}{4}(1+\xi)(1+\eta) & N_4 &= \frac{1}{4}(1-\xi)(1+\eta) \end{aligned} \qquad \text{... (3-18)}$$

Displacements of a point are interpolated from nodal d.o.f. by use of the same shape functions:

$$u = \sum N_i u_i \qquad v = \sum N_i v_i \qquad \text{... (3-19)}$$

Displacements u and v are parallel to the X and Y axes and not ξ and η axes.In order to write the strain-displacement matrix $[B]$, we must establish the relation between gradients in the two coordinate systems. Consider one of these gradients, the strain $\varepsilon_X = \partial u/\partial X$. We cannot immediately write the result because u is defined as a function of ξ and η rather than a function of X and Y . The chain rule can be applied to write:

$$\begin{Bmatrix} \frac{\partial u}{\partial \xi} \\ \frac{\partial v}{\partial \eta} \end{Bmatrix} = \begin{bmatrix} \frac{\partial X}{\partial \xi} & \frac{\partial Y}{\partial \xi} \\ \frac{\partial X}{\partial \eta} & \frac{\partial Y}{\partial \eta} \end{bmatrix} \begin{Bmatrix} \frac{\partial u}{\partial X} \\ \frac{\partial u}{\partial Y} \end{Bmatrix} \quad \text{or} \quad \begin{Bmatrix} \frac{\partial u}{\partial \xi} \\ \frac{\partial v}{\partial \eta} \end{Bmatrix} = [J] \begin{Bmatrix} \frac{\partial u}{\partial X} \\ \frac{\partial u}{\partial Y} \end{Bmatrix} \qquad \text{... (3-20)}$$

where $[J]$ is called the Jacobian matrix. Coefficients of $[J]$ can be obtained from Eq. 3-17:

$$\frac{\partial X}{\partial \xi} = \sum \frac{\partial N_i}{\partial \xi} X_i \ , \qquad \frac{\partial Y}{\partial \xi} = \sum \frac{\partial N_i}{\partial \xi} Y_i \ , \qquad \text{etc.} \qquad \text{... (3-21)}$$

Eq. (3-20) can be solved for the vector on the right-hand side. Hence strain ε_X becomes:

$$\varepsilon_X = \frac{\partial u}{\partial X} = J_{11}^* \frac{\partial u}{\partial \xi} + J_{12}^* \frac{\partial u}{\partial \eta} \qquad \text{... (3-22)}$$

where J_{11}^* and J_{12}^* are coefficients in the first row of $[J]^{-1}$ and:

$$\frac{\partial u}{\partial \xi} = \sum \frac{\partial N_i}{\partial \xi} u_i \qquad \text{and} \qquad \frac{\partial u}{\partial \eta} = \sum \frac{\partial N_i}{\partial \eta} u_i \qquad \text{... (3-23)}$$

The remaining strains ε_Y and γ_{XY} are formulated in a similar fashion, and at last the strain-displacement matrix $[B]$ can be written.

The element stiffness matrix is:

$$k = \int [B]^T [E][B] dV = \int_{-1}^{1}\int_{-1}^{1} [B]^T [E][B] t|J| d\xi d\eta \qquad \text{... (3-24)}$$

where t is element thickness and $|J|$ is the determinant of $[J]$. $|J|$ can be regarded as a scale factor between areas in the two coordinate systems, that is $dXdY = |J| d\xi d\eta$.

3.3.4 Gauss Quadrature

Integration for finding element stiffness matrix (Eq. 3-24) is seldom done and even possible analytically. Numerical techniques are usually employed the most common of which is the *Gauss quadrature*. In one-dimensional problems, Gauss quadrature evaluates the integral of a function as the sum of a number of terms:

$$I = \int_{-1}^{1} \phi d\xi \approx \sum_{i=1}^{n} W_i \phi_i \qquad \text{... (3-25)}$$

where W_i is a "weight" and ϕ_i is the value of $\phi = \phi(\xi)$ at a particular location often called a "Gauss point". Fig. 3-2 shows examples of this process for Gauss rules of orders $n = 1$, $n = 2$ and $n = 3$. Gauss points are at $\xi = 0$, $\xi = \pm a$, and $\xi = 0, \pm b$ respectively. There exist tabulations of Gauss point locations and the corresponding weights for values of n larger than 3. If $\phi = \phi(\xi)$ is a polynomial, n-point Gauss quadrature yields the exact integral if ϕ is of degree $2n-1$ or less.

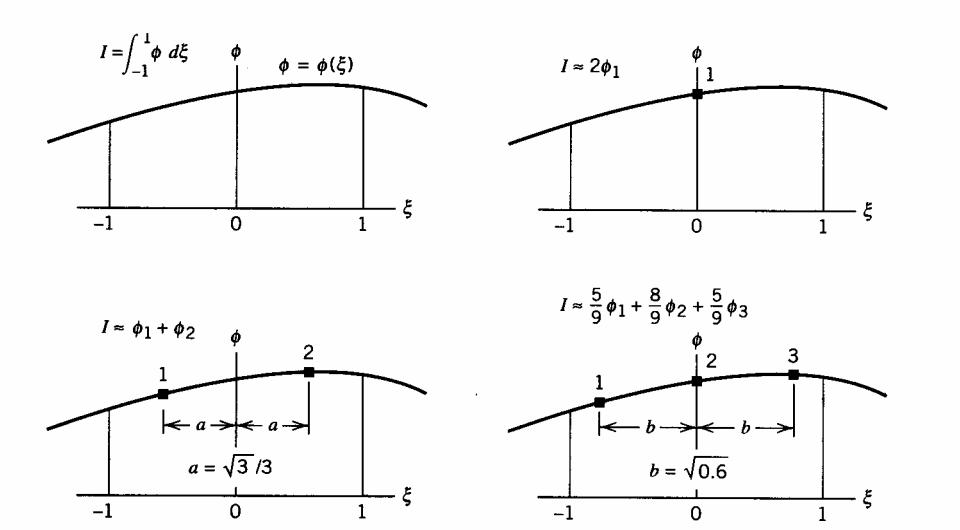

Fig. 3-2 One Dimensional Gauss Quadrature of Orders 1, 2, and 3 [10].

In two dimensions, integration is over a quadrilateral and a Gauss rule of order n uses n^2 points. The Gauss quadrature formula becomes:

$$I = \int_{-1}^{1}\int_{-1}^{1} \phi(\xi,\eta) d\xi d\eta \approx \sum_{i=1}^{n}\sum_{j=1}^{n} W_i W_j \phi(\xi_i, \eta_j) \qquad \text{... (3-26)}$$

where $W_i W_j$ is the product of one-dimensional weights. Usually $n = m$, i.e., the same number of points are used in each direction. Analogous Gauss quadrature rule can be written in three dimensions.

A finite element solution is usually inexact, and usually it errs by being too stiff. Overstiffness is usually made worse by using more Gauss points to integrate element stiffness matrices because additional points capture more higher-order terms in $[k]$. These terms resist some deformation modes that lower-order terms do not, and therefore act to stiffen the element. Accordingly, greater accuracy in the integration of $[k]$ usually produces less accuracy in the FE solution, in addition to requiring more computation.

On the other hand, use of too few Gauss points produces an even worse situation known by various names: instability, spurious singular mode, mechanism, kinematic mode, zero-energy mode, and hourglass mode. Instability occurs if one or more deformation modes happen to display zero strain at all Gauss points.

3.3.5 Nature of Finite Element Solutions

In the exact solution, according to the theory of elasticity, every differential element of a continuum is in static equilibrium, and compatibility prevails everywhere. An approximate finite element solution does not fulfill these requirements in every sense.

The nature of finite element solution with respect to equilibrium and compatibility at nodes, across interelement boundaries, and within individual elements is as follows [9].

1. Equilibrium of nodal forces and moments is satisfied.
2. Compatibility prevails at the nodes.
3. Equilibrium is usually not satisfied across interelement boundaries.
4. Compatibility may or may not be satisfied across interelement boundaries.
5. Equilibrium is usually not satisfied within elements.
6. Compatibility is satisfied within elements.

3.4 CONSTRAINT EQUATIONS

A constraint either prescribes the value of a d.o.f. (as in imposing a support condition) or prescribes a relationship among d.o.f [10]. In common terminology, a *single-point constraint* sets a single d.o.f. to a known value (often zero), and a *multi-point constraint* (MPC) imposes a relationship between two or more d.o.f. The constraint is called homogeneous if, upon transferring all terms that depend on displacement components to the left-hand side, the right-hand side - the "prescribed value" - is zero. It is called non-homogeneous otherwise. The constraint is called linear if all displacement components appear linearly on the left-hand-side, and nonlinear otherwise.

MPC commonly arise in a finite element formulation when one attempts to join elements of different dimension such as beam element and plane stress element (Fig. 3-3). Dissimilar elements cannot be simply joined directly. In the example of Fig. 3-3 direct joining is not possible because a plane beam element has two translational and one rotational d.o.f. at a given node while a plane stress element has only two translational d.o.f. Thus if one attempts direct connection by simply adding the stiffnesses of the beam and the plane stress element, recognizing only the sameness of the translational d.o.f. at the point of connection, correct coupling will not be achieved. The reason is that there is no moment communication between the beam element and the plane stress element, effectively rendering the connection between the beam and the plane stress element a hinge. One approach to solve such problems is by employing constraint equations.

The simplest and most commonly used technique is to form the constraint equations assuming rigid body kinematics. This approach does not yield stresses and displacements in accordance with the theory of elasticity. In this thesis work, constraints equations will be derived by equating work on either side of the mixed dimensional interface. This approach yields stresses and displacements in agreement to that predicted by theory of elasticity.

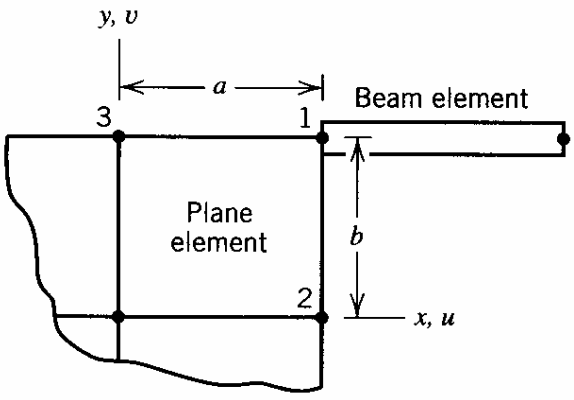

Fig. 3-3 A Plane Beam Element Joined to a Plane Quadrilateral Element [10].

Once the constraint equations have been developed, they have to be somehow incorporated in the finite element formulation.

The problem of incorporating constraint equations in the finite element formulation is a mathematical one for which there are a number of standard techniques. The three most common methods are: *Transformation*, *Lagrange Multiplier*, and *Penalty Function* techniques. Each method will be described next.

3.4.1 Transformation Method

Let the constraint equations that couple d.o.f. in $\{D\}$ be defined by:

$$[C]\{D\} = \{Q\} \qquad \text{... (3-27)}$$

where $[C]$ and $\{Q\}$ contain constants. Let's consider the most common case $\{Q\} = \{0\}$. Let Eq. 3-27 be partitioned so that:

$$[C_r \quad C_c]\begin{Bmatrix} D_r \\ D_c \end{Bmatrix} = \{0\} \qquad \text{... (3-28)}$$

where $\{D_r\}$ and $\{D_c\}$ are,respectively , d.o.f. to be determined and d.o.f. to be eliminated or "condensed out". Because there are as many d.o.f. $\{D_c\}$ as there are independent equations of constraint in Eq. 3-28, matrix $[C_c]$ is square and non-singular. Solution for $\{D_c\}$ yields:

$$\{D_c\} = [C_{rc}]\{D_r\}, \qquad \text{where} \quad [C_{rc}] = -[C_c]^{-1}[C_r] \qquad \text{... (3-29)}$$

We now write as one relation the identity $\{D_r\} = \{D_r\}$, and Eq. 3-29:

$$\begin{Bmatrix} D_r \\ D_c \end{Bmatrix} = [T]\{D_r\}, \qquad \text{where} \quad [T] = \begin{bmatrix} I \\ C_{rc} \end{bmatrix} \qquad \text{... (3-30)}$$

With the transformation matrix $[T]$ now defined, the familiar transformations $\{R\}=[T]^T\{R'\}$ and $[K]=[T]^T[K'][T]$ can be applied to the structural equations $[K']\{D'\}=\{R'\}$, which are partitioned as:

$$\begin{bmatrix} K_{rr} & K_{rc} \\ K_{cr} & K_{cc} \end{bmatrix} \begin{Bmatrix} D_r \\ D_c \end{Bmatrix} = \begin{Bmatrix} R_r \\ R_c \end{Bmatrix} \qquad \text{... (3-31)}$$

The condensed system is:

$$\left[K_{rr} + K_{rc}C_{rc} + C_{rc}^T K_{cr} + C_{rc}^T K_{cc} C_{rc}\right]\{D_r\} = \left\{R_r + C_{rc}^T R_c\right\} \qquad \text{... (3-32)}$$

After Eq. 3-32 is solved for $\{D_r\}$, Eq. 3-29 yields $\{D_c\}$. If $\{Q\} \neq \{0\}$ in Eq. 3-27, additional terms appear on the right side of Eq. 3-32.

3.4.2 Lagrange Multipliers

Lagrange's method of undetermined multipliers is used to find the maximum or minimum of a function whose variables are not independent but have some prescribed relation. In structural mechanics the function is potential energy Π_p and the variables are d.o.f. in $\{D\}$. System unknowns become $\{D\}$ and the Lagrange multipliers.

The procedure of Lagrange multipliers to impose constraints in finite element method is as follows. First the constraint equation is written as a homogeneous equation $[C]\{D\}-\{Q\}=\{0\}$. The left-hand side is multiplied by a row vector $\{\lambda\}^T$ that contains as many Lagrange multipliers λ_i as there as constraint equations. Next the result is added to the expression for potential energy:

$$\Pi_p = \frac{1}{2}\{D\}^T[K]\{D\} - \{D\}^T\{R\} + \{\lambda\}^T([C]\{D\}-\{Q\}) \qquad \text{... (3-33)}$$

Since the expression on the parenthesis is zero, nothing has been added to Π_p. Next the principle of stationary potential energy is invoked by writing $\{\partial \Pi_p / \partial D\} = \{0\}$ and $\{\partial \Pi_p / \partial \lambda\} = \{0\}$ from which:

$$\begin{bmatrix} K & C^T \\ C & 0 \end{bmatrix} \begin{Bmatrix} D \\ \lambda \end{Bmatrix} = \begin{Bmatrix} R \\ Q \end{Bmatrix} \quad \text{... (3-34)}$$

Eq. (3-34) is solved for both $\{D\}$ and $\{\lambda\}$.

3.4.3 Penalty Functions

If the constraint equation $[C]\{D\} = \{Q\}$ is written in the form:

$$\{t\} = [C]\{D\} - \{Q\} \quad \text{... (3-35)}$$

then $\{t\} = \{0\}$ implies the satisfaction of the constraints. The usual potential Π_p of a structural system can be augmented by a penalty function $\{t\}^T [\alpha]\{t\}/2$ where $[\alpha]$ is a diagonal matrix of "penalty numbers" α_i. Thus:

$$\Pi_p = \frac{1}{2}\{D\}^T [K]\{D\} - \{D\}^T \{R\} + \frac{1}{2}\{t\}^T [\alpha]\{t\} \quad \text{... (3-36)}$$

Next we substitute Eq. (3-35) into Eq. (3-36) and write the condition $\{\partial \Pi_p / \partial D\} = \{0\}$ to get:

$$\left([K] + [C]^T [\alpha][C]\right)\{D\} = \{R\} + [C]^T [\alpha]\{Q\} \quad \text{... (3-37)}$$

in which $[C]^T[\alpha]\{Q\}$ can be called the *penalty matrix*. If $[\alpha]=[0]$, the constraints are ignored. As $[\alpha]$ grows, $\{D\}$ changes in such a way that the constraint equations are more easily satisfied. The analyst is responsible for selecting appropriate numerical values of the α_i.

In comparison with Lagrange multipliers, penalty functions have the advantage of introducing no new variables. However, the penalty matrix may significantly increase the bandwidth (or wave front) of the structural equations depending on how the d.o.f. are numbered and what d.o.f. are coupled by the constraint equation. Penalty functions have the disadvantage of that penalty numbers must be chosen in an allowable range: large enough to be effective but not so large as to result in numerical difficulties.

Chapter 4
Mixed Dimensional Finite Element Modeling

4.1 INTRODUCTION

Efficiency and accuracy are two conflicting goals in most significantly large finite element problems. Ideally all the behavior of structures could be accurately predicted by modeling them as solid elements. However, this would result in excessively large computational effort rendering the project too costly. Thus, whenever possible, structures and structural members are represented by simpler models such as beams, plane stress/ strain, plates or shells. Such simplifications aid in better understanding of response and conceptual design in addition to reducing the computational effort significantly.

In most practical problems there are areas of the model that are an ideal candidate for dimensional reduction, but are bounded by areas that contain complex configurations such as discontinuities in geometry, loading, boundary conditions or material behavior. In many finite element analyses, reduced element types are thus combined with higher dimensional element types in a single model. In order to achieve a state of compatibility of displacements and stress equilibrium at the transition between dissimilar elements, some scheme is required to couple the differing element types in a manner that conforms to the theory of elasticity.

In many applications there are long slender regions, thin zones and complex chunky portions. Long slender regions can be represented appropriately using beam elements, thin zones can usually be modeled using shell elements, and chunky portions are best represented as three-dimensional elements. However, practical models usually contain a mixture of more than of the above regions. In order that each region is represented by an appropriate element type, some sort of coupling scheme is required to form a link between meshes of different type.

Kinematic coupling or *rigid linking* is the most basic and widely used method of coupling meshes of dissimilar elements. The method is simple to apply but is not appropriate as it results in a considerable stress disturbance at the transition.

Mixed-dimensional coupling using constraint equations has been shown to give stress distribution at the transition in agreement with the theory of elasticity [11]. In this approach constraint equations based on constraint equations derived by equating the work done on either side of the interface. This coupling technique does not result in stress disturbances at the transition.

In this investigation the analysis of moment frames with RBS connections as mixed dimensional model of beams and shells will be presented. The connection zone including the RBS is modeled by shell elements, while the portion of beams and columns away from the connection is modeled by beam elements. Coupling shall be achieved using multi-point constraint derived by equating the work done on the beam and shell sides of the interface. This approach is believed to balance accuracy and efficiency. Modeling of moment framed with RBS by prismatic frame model is quite inaccurate, while full shell or solid model of moment frames with RBS is computationally inhibiting and does not justify the gain on accuracy. The mixed dimensional beam-shell model while being nearly as accurate as the full shell model incurs a relatively small additional computational effort over the full frame model. In other words, the increase in accuracy as we go from the frame model to the mixed dimensional model is so substantial as to justify the corresponding increment in computation.

The derivation of constraint equations for general beam-shell coupling will follow. In Chapter 5 the beam-shell coupling technique will be applied to the particular case of moment frames with RBS connection.

4.2 BEAM-SHELL COUPLING

The general method of coupling elements of dissimilar dimension via constraint equations has been devised by McCune and applied by Monaghan [11]. The method is based on equating the work on both sides of the interface between elements of different dimensions. Six constraint equations are derived corresponding to each action (axial force, two bending moments, two shear forces and torsion).

4.2.1 Axial Force

The aim is to couple the axial displacements of the shell nodes at the transition to the axial displacements of the beam nodes such that the distribution of stress on the interface is similar to that given by elastic theory.

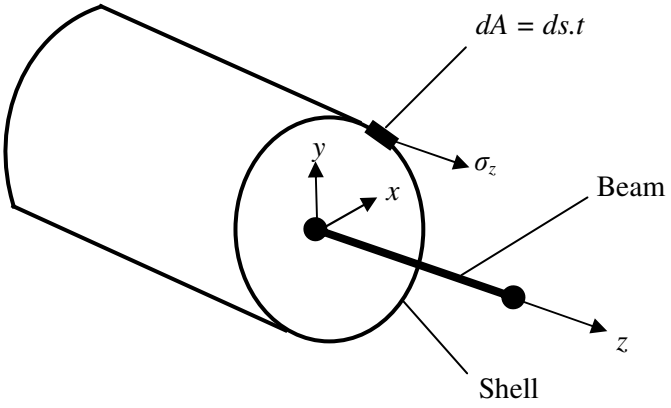

Fig. 4-1 Beam-Shell Coupling

Under the influence of axial force alone, the only non-zero stress on the shell side is the direct stress σ_z. Equating the work done by the 1D beam with the work done by the surface stress of the shell, the following equation results for the coordinate system shown in Fig. 4-1:

$$F_z w = \int_A \sigma_z W dA = \int_S \sigma_z t ds \quad \text{... (4-1)}$$

If the shell region is long slender, then the axial stress is uniform over the cross-section and is given by:

$$\sigma_z = \frac{F_z}{A} \quad \text{... (4-2)}$$

In the finite element model, the axial displacement at any point, in terms of the nodal displacements, $\{W\}$, and 1D shape functions, $[N]$, is:

$$W = [N]\{W\} \quad \text{... (4-3)}$$

This implies:

$$F_z w = \frac{F_z}{A} \sum_{i=1}^{Nelements} \int_{A_i} [N] dA \{W\} \quad \text{... (4-4)}$$

$$w = \frac{1}{A} \sum_{i=1}^{Nelements} \int_{l_i} t[N] dl \{W\} \quad \text{... (4-5)}$$

where t is the shell thickness and l is the element edge length. Since the implied element edge is simply the product of edge length and shell thickness:

$$\left(\sum_{j=1}^{Nelements} t_j l_j \right) w = \sum_{i=1}^{Nelements} \int_{l_i} t[N] dl \{W\} = [B]\{W\} \quad \text{... (4-6)}$$

Displacements compatibility between 1D element and the adjacent shell element edges can therefore be enforced as a multi-point constraint equation of the form:

$$-a_o w + B_1 W_1 + B_2 W_2 + B_3 W_3 + ... = 0 \qquad \text{... (4-7)}$$

4.2.2 Bending Moments

Under the influence of a pure bending moment, the only non-zero stress on the shell side of the transition is direct stress σ_z which varies linearly over the cross-section. The normal stress distribution due to a moment about the *x*-axis M_x with respect to the coordinate system shown in Fig. 1 is given by:

$$\sigma_z = (Px + Qy)M_x \qquad \text{... (4-8)}$$

where $P = \dfrac{I_{xy}}{I_{xy}^2 - I_{xx} I_{yy}}$ and $Q = \dfrac{I_{yy}}{I_{xx} I_{yy} - I_{xy}}$

This stress distribution will produce axial force and bending moments along the shell edge. At a given point on the shell edge, the axial force N_x, and the bending moments about the *x*-axis, M_{sx}, and *y*-axis, M_{sy}, per unit length of shell edge are given by:

$$\begin{aligned} N_{sx} &= \sigma_z t \\ M_{sx} &= \int_{-t/2}^{t/2} \sigma_z y dy = \int_{-t/2}^{t/2} (Px + Qy) M_x y dy = 2M_x Q \int_0^{t/2} y^2 dy = \frac{Qt^3}{12} M_x \\ M_{sy} &= \int_{-t/2}^{t/2} \sigma_z x dx = \int_{-t/2}^{t/2} (Px + Qy) M_x x dx = 2M_x P \int_0^{t/2} x^2 dx = \frac{Pt^3}{12} M_x \end{aligned} \qquad \text{... (4-9)}$$

Equating work on either side of the interface, we get:

$$M_x\theta_{x,beam} = \int_S N_{sx} W ds + \int_S M_{sx}\theta_x dx + \int_S M_{sy}\theta_y dy$$

$$M_x\theta_{x,beam} = \int_S (Px+Qy) M_x W t ds + \int_S \left(\frac{Qt^3}{12} M_x\right)\theta_x dx + \int_S \left(\frac{Pt^3}{12} M_x\right)\theta_y dy \quad \text{... (4-10)}$$

$$\theta_{x,beam} = \int_S (Px+Qy) W ds + \int_S \frac{Qt^3}{12}\theta_x dx + \int_S \frac{Pt^3}{12}\theta_y dy$$

In isoparametric finite element formulation, the translations and rotations are interpolated from nodal values using the same function $[N]$ as follows:

$$W = [N]\{W_i\} \qquad \theta_x = [N]\{\theta_{x,i}\} \qquad \theta_y = [N]\{\theta_{y,i}\} \quad \text{... (4-11)}$$

Substituting Eq. 4-11 into Eq. 4-10, we get the following constraint equation for bending about the *x*-axis:

$$\theta_{x,beam} = \int_S (Px+Qy)[N]\{W_i\} ds + \int_S \frac{Qt^3}{12}[N]\{\theta_{x,i}\} dx + \int_S \frac{Pt^3}{12}[N]\{\theta_{y,i}\} dy \quad \text{... (4-12)}$$

Bending about the *y*-axis produces a normal stress distribution given by:

$$\sigma_z = (Rx+Sy) M_y \quad \text{... (4-13)}$$

where $R = \dfrac{I_{xx}}{I_{xy}^2 - I_{yy} I_{xx}}$ and $S = \dfrac{I_{xy}}{I_{yy} I_{xx} - I_{xy}^2}$.

Analysis similar to that of bending about the *x*-axis gives the following constraint equation for bending about the *y*-axis:

$$\theta_{y,beam} = \int_S (Rx+Sy)[N]\{W_i\} ds + \int_S \frac{St^3}{12}[N]\{\theta_{x,i}\} dx + \int_S \frac{Rt^3}{12}[N]\{\theta_{y,i}\} dy \quad \text{... (4-14)}$$

Eq. 4-12 and Eq. 4-14 will result in two constraint equations of the form:

$$-\theta_{x,beam} + B_1 W_1 + B_2 W_2 + ... + C_1 \theta_{x,1} + C_2 \theta_{x,2} + ... + D_1 \theta_{y,1} + D_2 \theta_{y,2} + ... = 0 \quad \text{... (4-15a)}$$

$$-\theta_{y,beam} + E_1 W_1 + E_2 W_2 + ... + F_1 \theta_{x,1} + F_2 \theta_{x,2} + ... + G_1 \theta_{y,1} + G_2 \theta_{y,2} + ... = 0 \quad \text{... (4-15b)}$$

4.2.3 Shear Forces

For a shear force acting in the *y*-direction, the following constraint equation may be written:

$$F_y v = \int_A \tau_{xz} U dA + \int_A \tau_{yz} V dA \quad \text{... (4-16)}$$

Noting that for thin walled sections, the shear stress can be assumed to be constant, we can write $dA = tds$ in the above. Also U and V are interpolated from nodal values using the shape function $[N]$:

$$F_y v = \int_S \tau_{xz} [N]\{U_i\} t ds + \int_S \tau_{yz} [N]\{V_i\} t ds \quad \text{... (4-17)}$$

Similarly for shear force in the *x*-direction, we find:

$$F_x u = \int_S \tau_{xz} [N]\{U_i\} t ds + \int_S \tau_{yz} [N]\{V_i\} t ds \quad \text{... (4-18)}$$

Eq. 4-17 and Eq. 4-18 give two linear multi-point constraints of the form:

$$-v + B_1 U_1 + B_2 U_2 + ... + C_1 V_1 + C_2 V_2 + ... = 0 \quad \text{... (4-19a)}$$

$$-u + D_1 U_1 + D_2 U_2 + ... + E_1 V_1 + E_2 V_2 + ... = 0 \quad \text{... (4-19b)}$$

Shear force distribution as a result of a given shear force need to be found. For the purpose of this thesis work, shear stress distribution in accordance to classical beam theory will be found to give acceptable results.

4.2.4 Torsion

Torsional moment M_z will result in stresses τ_{xz} and τ_{yz} over a cross-section of a prismatic beam. The statement of work-equation becomes:

$$M_z\theta_z = \int_A \tau_{xz} U dA + \int_A \tau_{yz} V dA \qquad \text{... (4-20)}$$

After the distribution of the stresses τ_{xz} and τ_{yz} has been found, the above equation will result in a constraint equation of the form:

$$-\theta_z + B_1 U_1 + B_2 U_2 + ... + C_1 V_1 + C_2 V_2 + ... = 0 \qquad \text{... (4-21)}$$

Finding the actual stress distribution due to an applied torsion is not an easy task. Closed form solution using methods of theory of elasticity (such as stress function or the warping function approaches) is possible in only limited cases. A more general solution can be obtained by solving numerically solving the resulting Poisson equation.

Thus, six constraint equations for beam-shell coupling can be derived corresponding to each action. The equations can then be incorporated in the finite element formulation using either the Lagrange or the penalty method.

Chapter 5
Beam-Shell Model of Frames with RBS Connections

5.1 INTRODUCTION

Derivation of five equations corresponding to axial force, shear force, and bending moment will now be given. In the derivation, four node isoparametric shell element shall be assumed. The cross-sectional properties of an I-section are as shown in Fig. 5-1.

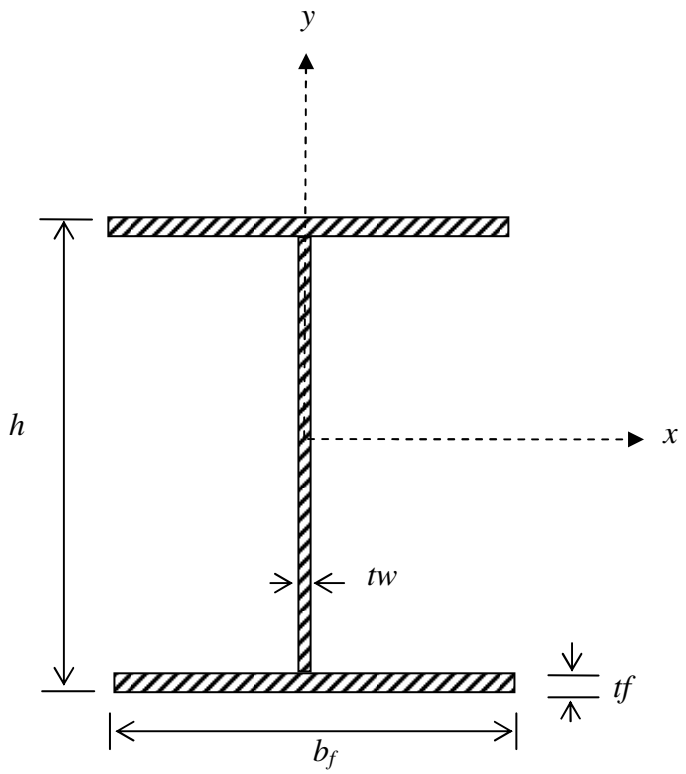

Fig. 5-1 Cross-sectional Parameters of I Beam Section

5.2 AXIAL FORCE

From Eq. (4-6) we have:

$$\left(\sum_{j=1}^{Nelements} t_j l_j \right) w = \sum_{i=1}^{Nelements} \int_{l_i} t[N] dl \{W\} = [B]\{W\} \quad \text{... (5-1)}$$

Consider the wide flange I-section shown in Fig. 5-2.

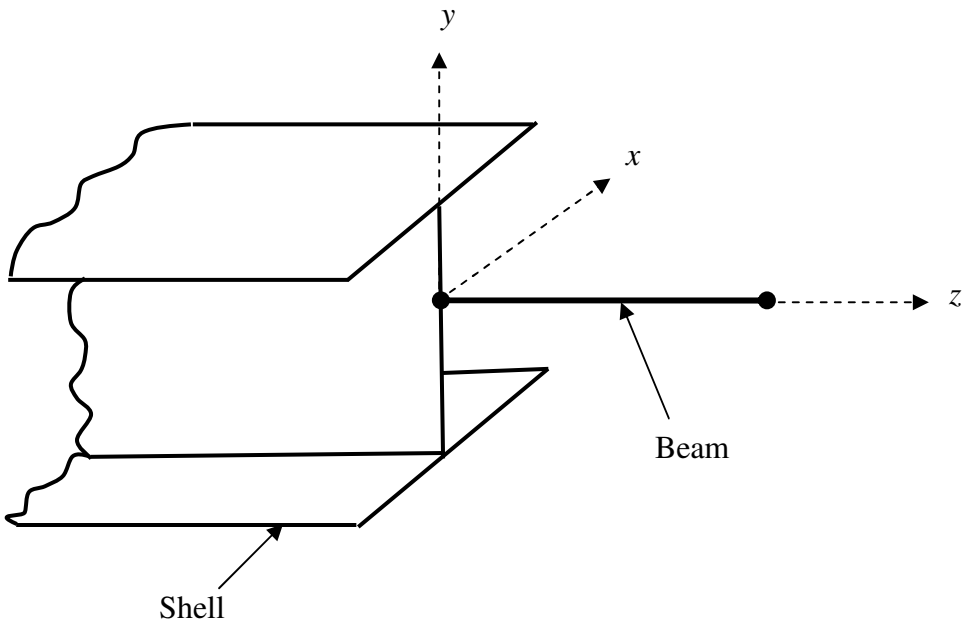

Fig. 5-2 Beam-Shell Model of Wide Flange Beam

The I-section is meshed into four node isoparametric shell elements whose shape functions are given by:

$$N_i = \frac{1}{4}(1 \pm \xi)(1 \pm \eta) \quad \text{... (5-2)}$$

Coefficient of Beam Node:

$$\sum tl = 2t_f b_f + h_f t_w \quad \text{where} \qquad h_f = h - t_f \qquad \text{... (5-3)}$$

Flange Element:

Consider a typical flange element shown in Fig. 5-3 below.

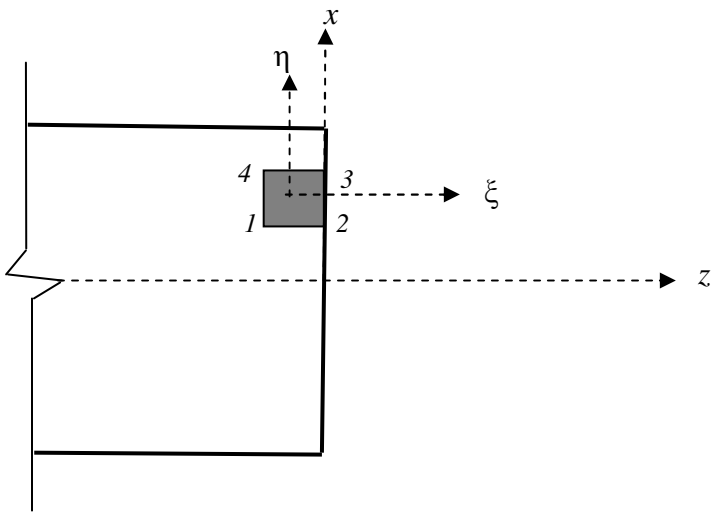

Fig. 5-3 Typical Flange Element

The shape functions now become:

$$\begin{aligned} N_1 &= 1/4\,(1-\xi)(1-\eta) \\ N_2 &= 1/4\,(1+\xi)(1-\eta) \\ N_3 &= 1/4(1+\xi)(1+\eta) \\ N_4 &= 1/4\,(1-\xi(1+\eta)) \end{aligned} \qquad \text{... (5-4)}$$

For the flange element shown in Fig. 5-3 above:

$$\int_{l_i} t[N]dl = t_f \int_{l_i} [N]dx = t_f \int_{l_i} [N]\frac{dx}{d\eta}d\eta = t_f \int_{-1}^{1} [N]Jd\eta \qquad \text{... (5-5)}$$

where $J = \dfrac{dx}{d\eta} = \dfrac{d}{d\eta}[N]\{x_i\}$.

Along edge 2-3 ($\xi = 1$): $[N] = \begin{bmatrix} 0 & \frac{1-\eta}{2} & \frac{1+\eta}{2} & 0 \end{bmatrix}$

Therefore $\frac{d}{d\eta}[N] = \begin{bmatrix} 0 & -\frac{1}{2} & \frac{1}{2} & 0 \end{bmatrix}$, and $J = \frac{dx}{d\eta} = \frac{d}{d\eta}[N]\{x_i\} = \frac{x_3 - x_2}{2} = \frac{\Delta x}{2}$.

Now $\int_{l_i} t[N]dl = \frac{t_f \Delta x}{2}\int_{-1}^{1}[N]d\eta\{W_i\} = \frac{t_f \Delta x}{2}[0 \quad 1 \quad 1 \quad 0]\begin{Bmatrix} W_1 \\ W_2 \\ W_3 \\ W_4 \end{Bmatrix} = \frac{t_f \Delta x}{2}(W_2 + W_3)$ ... (5-6)

Web Element:

Similar analysis on a typical web element gives:

$$\int_{l_i} t[N]dl = \frac{t_w \Delta y}{2}(W_2 + W_3) \qquad \text{... (5-7)}$$

Thus the constraint equation for axial force becomes:

$$(2t_f b_f + h_f t_w)w = \sum_{flange} \frac{t_f \Delta x}{2}(W_2 + W_3) + \sum_{web} \frac{t_w \Delta y}{2}(W_2 + W_3) \qquad \text{... (5-8)}$$

5.3 BENDING MOMENTS

5.3.1 Bending about x-axis

From Eq. (4-12) we have:

$$\theta_{x,beam} = \int_S (Px + Qy)[N]\{W_i\}tds + \int_S \frac{Qt^3}{12}[N]\{\theta_{x,i}\}dx + \int_S \frac{Pt^3}{12}[N]\{\theta_{y,i}\}dy \qquad \text{... (5-9)}$$

For an I-section shown in Fig. 5-2:

$$P = 0 \qquad Q = 1/I_{xx} \qquad \text{... (5-10)}$$

and the constraint equation can be written as:

$$\theta_{x,beam} = \sum_{i=1}^{Nelem}\left[\frac{t}{I_{xx}}\int_{l_i} y[N]ds\{W_i\} + \frac{t_f^{\,3}}{12I_{xx}}\int_{l_i}[N]dx\{\theta_{x,i}\}\right] \quad \text{or} \quad \text{... (5-11)}$$

$$I_{xx}\theta_{x,beam} = \sum_{i=1}^{Nelem}\left[t\int_{l_i} y[N]ds\{W_i\} + \frac{t_f^{\,3}}{12}\int_{l_i}[N]dx\{\theta_{x,i}\}\right] \quad \text{... (5-12)}$$

Flange Element:

For a flange element shown in Fig. 5-3:

$$t\int_{l_i} y[N]ds\{W_i\} = t_f\int_{l_i}(\pm h_f/2)[N]dx\{W_i\} = \pm t_f\frac{h_f}{2}\frac{\Delta x}{2}\int_{-1}^{1}[N]d\eta\{W_i\} = \pm\frac{t_f h_f \Delta x}{4}(W_2 + W_3) \quad \text{... (5-13a)}$$

$$\frac{t_f^{\,3}}{12}\int_{l_i}[N]dx\{\theta_{x,i}\} = \frac{t_f^{\,3}}{12}\frac{\Delta x}{2}\int_{-1}^{1}[N]d\eta\{\theta_{x,i}\} = \frac{t_f^{\,3}\Delta x}{24}(\theta_{x,2} + \theta_{x,3}) \quad \text{... (5-13b)}$$

Web Element:

Consider a typical web element shown in Fig. 5-4 below.

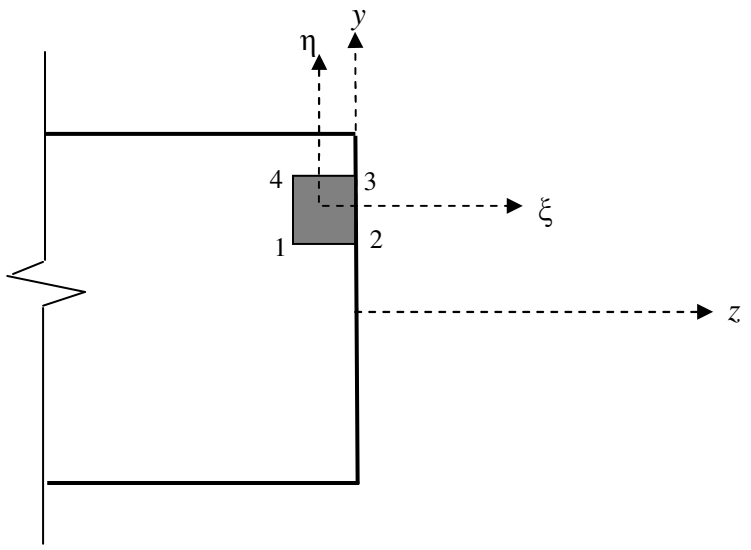

Fig. 5-4 Typical Web Element

$$t\int_{l_i} y[N]ds\{W_i\} = t_w \frac{\Delta y}{2}\int_{-1}^{1} y[N]d\eta\{W_i\} \quad \text{... (5-14)}$$

It can be shown that:

$$\int_{-1}^{1} y[N]d\eta\{W_i\} = \int_{-1}^{1}\{[N]\{y_i\}\}[N]d\eta\{W_i\} = \left(\frac{2y_2 + y_3}{3}\right)W_2 + \left(\frac{y_2 + 2y_3}{3}\right)W_3 \quad \text{... (5-15)}$$

Thus:

$$t\int_{l_i} y[N]ds\{W_i\} = t_w \frac{\Delta y}{2}\int_{-1}^{1} y[N]d\eta\{W_i\} = \frac{t_w \Delta y}{2}\left[\left(\frac{2y_2 + y_3}{3}\right)W_2 + \left(\frac{y_2 + 2y_3}{3}\right)W_3\right] \quad \text{... (5-16)}$$

Constraint equation for bending about the *x*-axis becomes:

$$I_{xx}\theta_{x,beam} = \sum_{flange}\left[\pm\frac{t_f h_f \Delta x}{4}(W_2 + W_3) + \frac{{t_f}^3 \Delta x}{24}(\theta_{x,2} + \theta_{x,3})\right] + \sum_{web}\left[\frac{t_w \Delta y}{2}(k_2 W_2 + k_3 W_3)\right]$$

where $k_2 = (2y_2 + y_3)/3$ and $k_3 = (y_2 + 2y_3)/3$ ... (5-17)

5.3.2 Bending about y-axis

Analogous constraint equation for bending about the *y*-axis can be written as:

$$I_{yy}\theta_{y,beam} = \sum_{flange}\frac{t_f \Delta x}{2}(k_2 W_2 + k_3 W_3) + \sum_{web}\frac{{t_w}^3 \Delta y}{24}(\theta_{y,2} + \theta_{y,3})$$

where $k_2 = (2x_2 + x_3)/3$ and $k_3 = (x_2 + 2x_3)/3$ ... (5-18)

5.4 SHEAR FORCES

5.4.1 Shear Force in the y-direction

Shear Stress Distribution

The shear stress distribution has been assumed in accordance to thin wall theories as shown in Fig. 5-5 [12].

$$\tau_{xz} = \tau_w = (m_1 - m_2 x)\frac{F_y}{I_{xx}} \qquad \text{... (5-19)}$$

where $m_1 = b_f\left(h^2 - h_w{}^2\right)/16t_f$ and $m_2 = \left(b_f{}^2 - h_w{}^2\right)/8t_f$

$$\tau_{yz} = \tau_f = \left(m_3 - m_4 y^2\right)\frac{F_y}{I_{xx}} \qquad \text{... (5-20)}$$

where $m_3 = \left(b_f h^2 - b_f h_w{}^2 + t_w h_w{}^2\right)/8t_w$ and $m_4 = 0.5$.

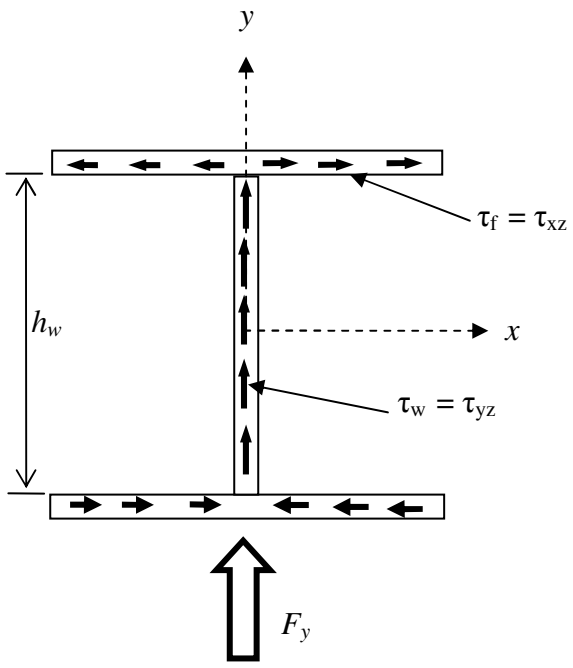

Fig. 5-5 Shear Stress Distribution due to Force in the Y-direction

Work equation:

$$F_y v_{beam} = \int_S \tau_{xz} U t dx + \int_S \tau_{yz} V t dy \qquad \text{... (5-21)}$$

Noting that $U = [N]\{U_i\}$ and $V = [N]\{V_i\}$, and using the thin-wall formulas:

$$F_y v_{beam} = \int_{flange} (m_1 - m_2 x)\frac{F_y}{I_{xx}}[N]\{U_i\} t dx + \int_{web} (m_3 - m_4 y^2)\frac{F_y}{I_{xx}}[N]\{V_i\} t dy \quad \text{or}$$

$$I_{xx} v_{beam} = \sum_{flange} \frac{t_f \Delta x}{2} \int_{-1}^{1} (m_1 - m_2 x)[N] d\eta \{U_i\} + \sum_{web} \frac{t_w \Delta y}{2} \int_{-1}^{1} (m_3 - m_4 y^2)[N] d\eta \{V_i\} \qquad \text{... (5-22)}$$

It can be shown that:

$$\int_{-1}^{1} (m_1 - m_2 x)[N] d\eta \{U_i\} = C_2 U_2 + C_3 U_3 \qquad \text{... (5-23)}$$

where $C_2 = m_1 - k_2 m_2$, $k_2 = (2x_2 + x_3)/3$ and
$C_3 = m_1 - k_3 m_2$, $k_3 = (x_2 + 2x_3)/3$

Also:

$$\int_{-1}^{1} (m_3 - m_4 y^2)[N] d\eta \{V_i\} = C_4 V_2 + C_5 V_3 \qquad \text{... (5-24)}$$

where $C_4 = m_3 - k_4 m_4$, $k_4 = \frac{1}{2} y_2{}^2 + \frac{2}{3} y_2 y_3 + \frac{1}{3} y_3{}^2$ and
$C_5 = m_3 - k_5 m_4$, $k_5 = \frac{1}{3} y_2{}^2 + \frac{2}{3} y_2 y_3 + \frac{1}{2} y_3{}^2$

Thus the constraint equation for shear force in the *y*-direction becomes:

$$I_{xx} v_{beam} = \sum_{flange} \frac{t_f \Delta x}{2}(C_2 U_2 + C_3 U_3) + \sum_{web} \frac{t_w \Delta y}{2}(C_4 V_2 + C_5 V_3) \qquad \text{... (5-25)}$$

5.4.2 Shear Force in the x-direction

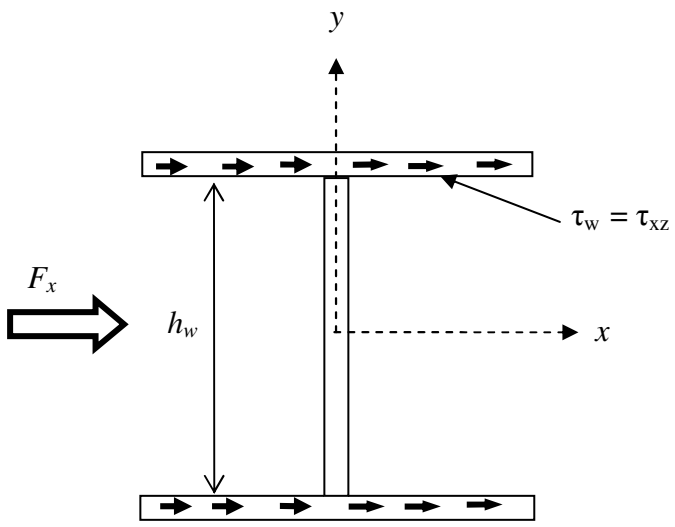

Fig. 5-6 Shear Stress Distribution due to Force in the X-direction

Shear stress distribution according to thin-wall theories (Fig. 5-6):

$$\tau_f = \tau_{xz} = \left(m_5 - m_6 x^2\right)\frac{F_x}{I_{yy}} \qquad \text{... (5-26)}$$

where $m_5 = \dfrac{{b_f}^2}{4}$ and $m_6 = 0.5$

The constraint equation for shear force in the *x*-direction becomes:

$$I_{yy} u_{beam} = \sum_{flange} \frac{t_f \Delta x}{2}\left(C_2 U_2 + C_3 U_3\right) \qquad \text{... (5-27)}$$

where $C_2 = m_5 - k_2 m_6$, $k_2 = \dfrac{1}{2}{x_2}^2 + \dfrac{2}{3}x_2 x_3 + \dfrac{1}{3}{x_3}^2$

$C_3 = m_5 - k_3 m_6$, $k_3 = \dfrac{1}{2}{x_3}^2 + \dfrac{2}{3}x_2 x_3 + \dfrac{1}{3}{x_2}^2$

A Fortran 90 program has been written to automate the beam-shell coupling for any wide-flange I-section. The program description and listing is given in Appendix A. Once the constraint equations are developed they can be incorporated in the finite element formulation using the transformation, Lagrange multipliers or the penalty function methods. Some commercial software such as ANSYS and ABAQUS allow the user to define multi-point constraints and solve the problem by incorporating internally the prescribed constraint equations. In the next chapter the validity of the derived constraint equations shall be illustrated using the general purpose finite element program ANSYS [13].

Chapter 6
Application of Constraint Equations

6.1 INTRODUCTION

In this chapter the validity of the derived constraint equations shall be demonstrated by specific examples using ANSYS [13]. The validity of a given set of constraint equations is shown by the fact there is no stress disturbance at the mixed-dimensional interface. Moreover, the validity of the constraint equations will be tested by comparing quantitatively the solution of the mixed dimensional model with that of full shell model of the problem and also with theoretical results whenever possible.

The region over which the shell model extends in the mixed model is an important issue that should be addressed. In this study no attempt shall be made to find the optimum length of the beam and column to be modeled by shell elements. However, for the examples considered the extent of the shell region will be varied.

Two examples shall be considered for the purpose of illustrating the application of the derived constraint equations. The first is a cantilever beam fixed at one end loaded by axial, couple or transverse load at the free end. The main purpose of this example is to illustrate that the constraint equations provide valid beam-shell coupling. Various lengths of the extent of the shell region are considered. The second example considered is an inverted-L frame. This example attempts to illustrate the applicability constraint equations in moment frames with RBS connections. It should be mentioned that it was not possible to include more realistic examples of moment frames for the reason that the available educational version of ANSYS does not allow solution beyond certain number of elements and nodes.

The shell region has been modeled using the four node ANSYS element SHELL63. The description of SHELL63 as obtained from ANSYS is given in Appendix B. Both membrane and bending capabilities of the element has been activated. It should be noted the derived constraint equations are element dependent and cannot be used with any element type such as a quadratic shell element.

6.2 EXAMPLE 1: CANTILEVER BEAM

The geometry and loading of the problem considered is shown in Fig. 6-1 below.

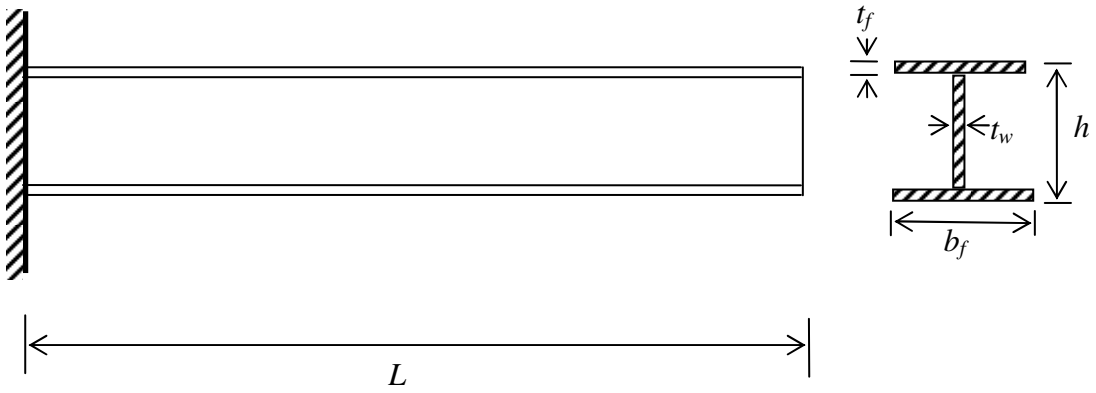

Fig. 6-1 Example 1: Cantilever Beam

The following geometric data has been considered.

L = 4.0 m

Beam Cross-section:

h = 533 mm
b_f = 330 mm
t_f = 22.0 mm
t_w = 13.4 mm

Material: E = 200 GPa , υ = 0.3

6.2.1 Cantilever without RBS

The cantilever beam of Example 1 is initially considered without RBS. The beam has been modeled as a full shell model and as a mixed beam-shell model. Different lengths of shell regions are considered in the mixed-dimensional models. Three loading cases are considered:

a. Axial Load: a tensile force of magnitude 10 kN applied at the free end.
b. Couple Load: a couple of magnitude 10 kN.m applied at the free end.
c. Transverse Load: a transverse force of magnitude 10 kN applied at the free end.

The details of full shell model and mixed model of the beam are discussed next.

Full Shell Model

The cantilever beam is modeled with 200 shell elements as shown in the Fig. 6-2. The full shell model is subjected to each of the above three loading cases and analyzed.

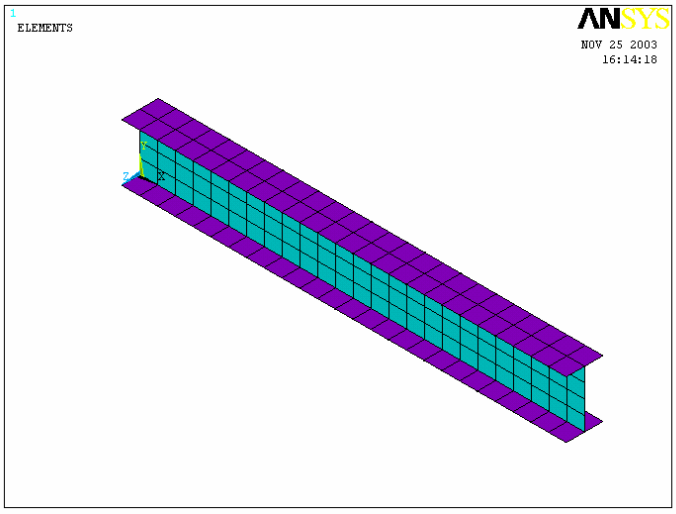

Fig. 6-2 Full Shell Model of Cantilever Beam without RBS

Mixed Model

The beam has also been modeled as a mixed beam-shell model. Coupling has been achieved via the constraint equations derived in Chapter 5. The length of the beam (starting from the fixed end) to be modeled by shell elements has been varied from 10% to 60% of beam length. An example of mixed model in which the shell region extends over 30 % of beam length is shown in Fig. 6-3 below. The mixed models are subjected to each of the three loading cases and analyzed.

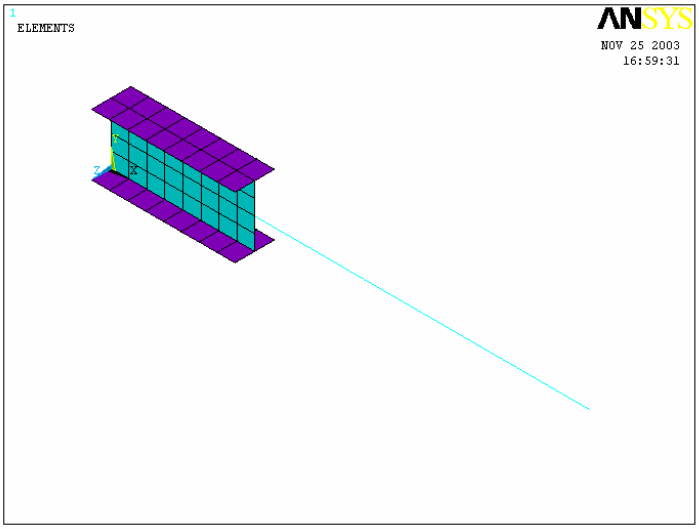

Fig. 6-3 Mixed Model of Cantilever Beam without RBS

Axial Load

An axial tensile force of 10 kN is applied at the free end of the cantilever beam. The resulting axial normal stress distribution is shown in Fig. 6-4. It can be seen that there is no stress disturbance at the mixed dimensional interface.

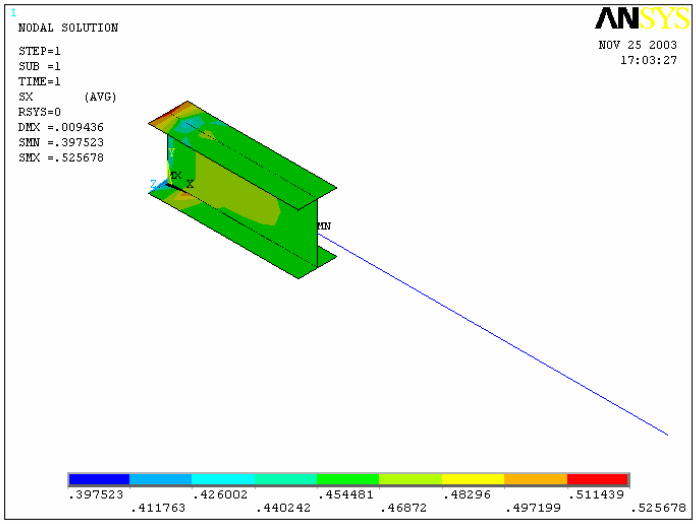

Fig. 6-4 Normal Stress Distribution of Cantilever without RBS under Axial Load

Couple Load

The mixed model is subjected to a couple of 10 kN-m at the free end and analyzed. The resulting normal stress distribution is shown in Fig. 6-5 below.

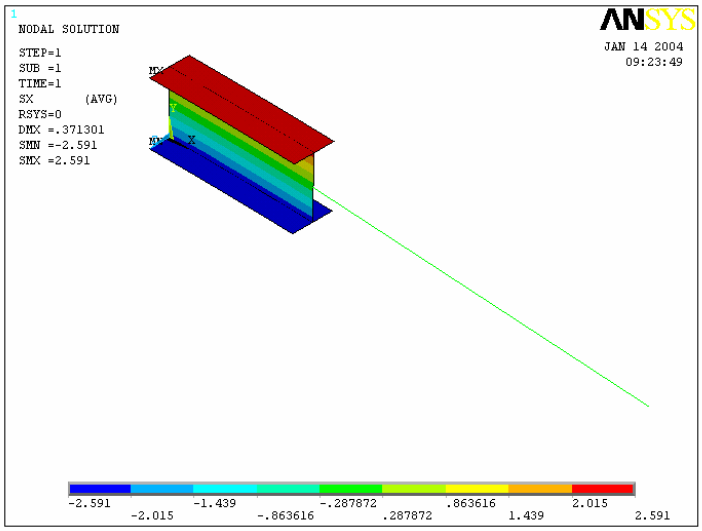

Fig. 6-5 Normal Stress Distribution of Cantilever without RBS under Couple Loading

Transverse Load

The mixed model is subjected to a transverse downward force of 10 kN at the free end and the resulting normal stress and shear stress distribution is shown in Fig. 6-6 and Fig. 6-7.

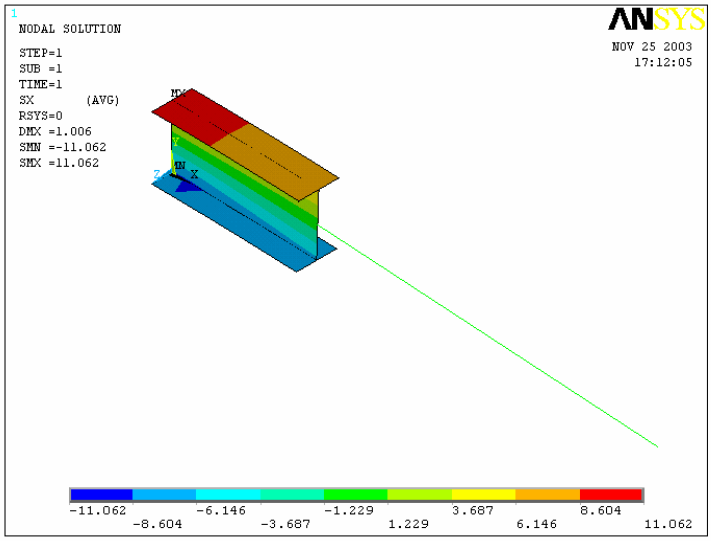

Fig. 6-6 Normal Stress Distribution of Cantilever without RBS under Transverse Load

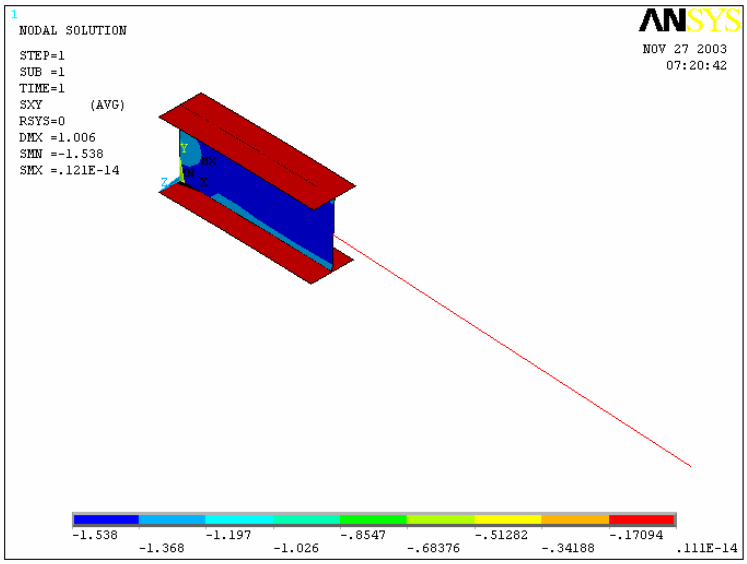

Fig.6-7 Shear Stress Distribution of Cantilever without RBS under Transverse Load

It can be seen that there is no stress disturbance at the mixed dimensional interface and the constraint equations derived in Chapter 5 yield valid transition between beam and shell elements for axial force, bending moments and shear force. The validity of the coupling will also be demonstrated by comparing stress and displacement outputs of the mixed models and full shell model at the mixed dimensional interface.

Comparison of Results at Mixed Dimensional Interface

It has been shown that there are no spurious stresses at the mixed dimensional interface which is an indication that the derived constraint equations provide valid beam-shell coupling. Now the validity of beam-shell coupling will be tested by comparing the results of the mixed model and the full shell model at the mixed dimensional interface. If the displacement and stress outputs at the beam-shell interface of the mixed model are the same or very close to those of the full model, it can be said that correct coupling has been achieved. The comparison shall be made at the dimensional interface for displacement and stress outputs at the nodes shown in Fig. 6-8.

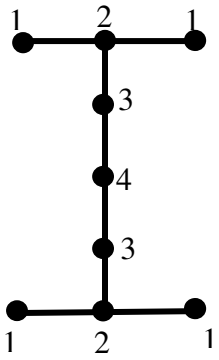

Fig. 6-8 Nodes at which Stress and Displacements Outputs are Compared.

The comparison of displacements and stresses at the mixed dimensional interface is made for mixed models in which the shell region extends over 20%, 40% and 60% of beam length. The comparisons corresponding to axial, couple and transverse loadings are shown in Table 6-1, Table 6-2 and Table 6-2, respectively, below. Note that Ux and Uy are axial and transverse displacements, respectively, and Sx is axial normal stress.

Table 6-1: Comparison of Displacements and Stresses at Interface - Axial Load

Shell 20% of Beam Length						
	Mixed Model		Full Shell		Percent Error	
Nodes	Ux (mm)	Sx (MPa)	Ux (mm)	Sx (MPa)	In Ux	In Sx
1	0.0018571	0.46748	0.0018563	0.46731	-0.043	-0.037
2	0.0018563	0.46786	0.0018558	0.46781	-0.027	-0.012
3	0.0018533	0.46867	0.0018548	0.46907	0.081	0.085
4	0.0018521	0.46916	0.0018544	0.46965	0.124	0.104
Shell 40% of Beam Length						
	Mixed Model		Full Shell		Percent Error	
Nodes	Ux (mm)	Sx (MPa)	Ux (mm)	Sx (MPa)	In Ux	In Sx
1	0.0037278	0.46800	0.0037278	0.46800	0	0
2	0.0037278	0.46800	0.0037278	0.46800	0	0
3	0.0037278	0.46801	0.0037278	0.46801	0	0
4	0.0037278	0.46801	0.0037278	0.46801	0	0
Shell 60% of Beam Length						
	Mixed Model		Full Shell		Percent Error	
Nodes	Ux (mm)	Sx (MPa)	Ux (mm)	Sx(MPa)	In Ux	In Sx
1	0.0055998	0.46800	0.0055998	0.46798	0	-0.0043
2	0.0055998	0.46800	0.0055998	0.46800	0	0.0000
3	0.0055998	0.46800	0.0055998	0.46803	0	0.0064
4	0.0055998	0.46800	0.0055998	0.46803	0	0.0064

Table 6-2: Comparison of Displacements and Stresses at Interface - Couple Load

Shell 20% of Beam Length						
	Mixed Model		Full Shell		Percent Error	
Nodes	Uy (mm)	Sx (MPa)	Uy(mm)	Sx (MPa)	In Uy	In Sx
1	0.014681	2.3676	0.014435	2.3280	1.704	-1.703
2	0.014871	2.36815	0.014622	2.3283	1.702	-1.712
3	0.014531	1.1838	0.014287	1.164	1.708	-1.701
4	0.014418	0	0.014176	0	1.707	0
Shell 40% of Beam Length						
	Mixed Model		Full Shell		Percent Error	
Nodes	Uy (mm)	Sx (MPa)	Uy (mm)	Sx(MPa)	In Uy	In Sx
1	0.058952	2.3679	0.057962	2.3281	1.708	-1.707
2	0.059142	2.3679	0.058148	2.3281	1.709	-1.708
3	0.058801	1.1839	0.057814	1.1641	1.707	-1.701
4	0.058688	0	0.057702	0	1.709	0
Shell 60% of Beam Length						
	Mixed Model		Full Shell		Percent Error	
Nodes	Uy (mm)	Sx (MPa)	Uy (mm)	Sx (MPa)	In Uy	In Sx
1	0.13288	2.3679	0.13065	2.3281	1.701	-1.707
2	0.13307	2.3679	0.13083	2.3281	1.712	-1.710
3	0.13273	1.1839	0.1305	1.1641	1.709	-1.701
4	0.13261	0	0.13039	0	1.703	0

Table 6-3: Comparison of Displacements and Stresses at Interface - Transverse Load

Shell 20% of Beam Length						
	Mixed Model		Full Shell		Percent Error	
Nodes	Uy (mm)	Sx (MPa)	Uy (mm)	Sx(MPa)	In Uy	In Sx
1	0.069413	7.7469	0.069421	7.449200	0.012	-4.00
2	0.070064	7.7654	0.070014	7.450675	-0.071	-4.22
3	0.069007	3.8837	0.068943	3.724600	-0.093	-4.27
4	0.068674	0	0.068587	0	-0.127	0.00
Shell 40% of Beam Length						
	Mixed Model		Full Shell		Percent Error	
Nodes	Uy (mm)	Sx (MPa)	Uy (mm)	Sx (MPa)	In Uy	In Sx
1	0.23144	5.8541	0.23202	5.5875	0.25	-4.77
2	0.23195	5.8700	0.23247	5.5875	0.22	-5.06
3	0.23116	2.9375	0.23116	2.7937	0.00	-5.15
4	0.23092	0	0.23140	0	0.21	0.00
Shell 60% of Beam Length						
	Mixed Model		Full Shell		Percent Error	
Nodes	Uy (mm)	Sx (MPa)	Uy(mm)	Sx (MPa)	In Uy	In Sx
1	0.46014	3.9597	0.46460	3.7250	0.96	-6.30
2	0.46049	3.9754	0.46490	3.7250	0.95	-6.72
3	0.45998	1.9901	0.46436	1.8625	0.94	-6.85
4	0.45983	0	0.46419	0	0.94	0.00

The percent error has been defined as:

$$\text{Percent Error} = \frac{\text{Full Shell Model Result} - \text{Mixed Model Result}}{\text{Full Shell Model Result}} \times 100$$

The percent error thus defined is a measure of the deviation of mixed model results from those of the full shell model at the beam-shell interface. It can be seen that the displacements and stresses at the dimensional interface of the mixed model are very close to the corresponding results in the full shell model. The maximum percent error in displacements is less than 2 %. This indicates that valid coupling has been achieved using the derived constraint equations.

Results of Elementary Mechanics of Materials

Axial Load

According to elementary mechanics of materials the tip displacement of a beam under axial loading is given by:

$$\Delta_{axial} = \frac{PL}{AE} = 0.0094910 \text{ mm} \quad \text{... (6-1)}$$

Couple Load

The transverse deflection as a result of an end couple is given by:

$$\Delta_{couple} = \frac{ML^2}{2EI} = 0.37070 \text{ mm} \quad \text{... (6-2)}$$

Transverse Load

The tip deflection consists of deformation due to flexure and shear. The tip deflection due to flexural deformations is given by:

$$\Delta_{flexure} = \frac{PL^3}{3EI} = 0.98854 \text{ mm} \quad \text{... (6-2)}$$

The tip deflection due to shear deformations is given by:

$$\Delta_{shear} = \frac{PL}{A_s G} = 0.02971 mm \quad \text{... (6-3)}$$

where G is the shear modulus and A_s is the *effective shear area* [See Appendix C].

The total tip deflection is:

$$\Delta_{total} = \Delta_{flexure} + \Delta_{shear} = 1.01816 \text{ mm}$$

Summary of Results

Next a summary of the results obtained using the full shell, mixed models and elementary mechanics of materials will be given. The tip deflection will be taken as the quantity of interest. For the full shell model, the tip deflection at a given section is taken as the average of the deflections of the five nodes at the section of the beam.

Table 6-4: Summary of Results of Cantilever Beam without RBS

Model	Shell Region (% of Beam Length)	Number of Shell Elements	Axial Tip Deflection (mm) (due to axial load of 10kN)	Transverse Tip Deflection (mm) (due to a couple load of 10kN.m)	Transverse Tip Deflection (mm) (due to a transverse load of 10 kN)
Beam	0	0	0.0094910	0.37070	1.01816
Mixed	10	24	0.0094627	0.37069	1.02140
Mixed	20	40	0.0094486	0.37121	1.02570
Mixed	30	64	0.0094358	0.37130	1.02690
Mixed	40	80	0.0094224	0.37079	1.02500
Mixed	50	104	0.0094095	0.36990	1.02130
Mixed	60	120	0.0093962	0.36855	1.01570
Shell	100	200	0.00937660	0.36424	1.04642

To study the effect of mesh density, the mixed models of the cantilever beam without RBS are considered with finer mesh. A summary of results of analysis with finer mesh is given in Table 6-5 below. It was not possible to analyze the full shell model with a finer mesh because of the limitations of the available ANSYS version.

Table 6-5: Summary of Results of Cantilever Beam without RBS using Finer Mesh

Model	Shell Region (% of Beam Length)	Number of Shell Elements	Axial Tip Deflection (mm) (due to axial load of 10kN)	Transverse Tip Deflection (mm) (due to a couple load of 10kN.m)	Transverse Tip Deflection (mm) (due to a transverse load of 10 kN)
Beam	0	0	0.0094910	0.37070	1.01816
Mixed	10	75	0.0094638	0.37084	1.0221
Mixed	20	150	0.0094506	0.37135	1.0261
Mixed	30	225	0.0094375	0.37136	1.0269
Mixed	40	300	0.0094244	0.37086	1.0249
Mixed	50	375	0.0094113	0.36985	1.0205
Mixed	60	450	0.0093982	0.36628	1.0141

The results are presented as a plot of tip deflection versus the extent of shell region in Fig. 6-9, Fig. 6-10 and Fig. 6-11 below.

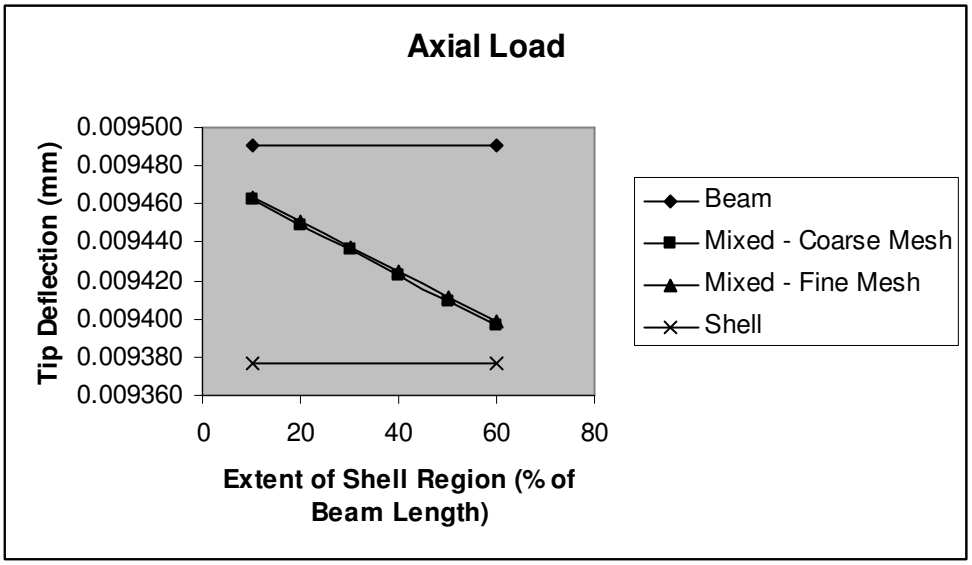

Fig. 6-9 Tip Deflection vs. Extent of Shell Region for Axial Load

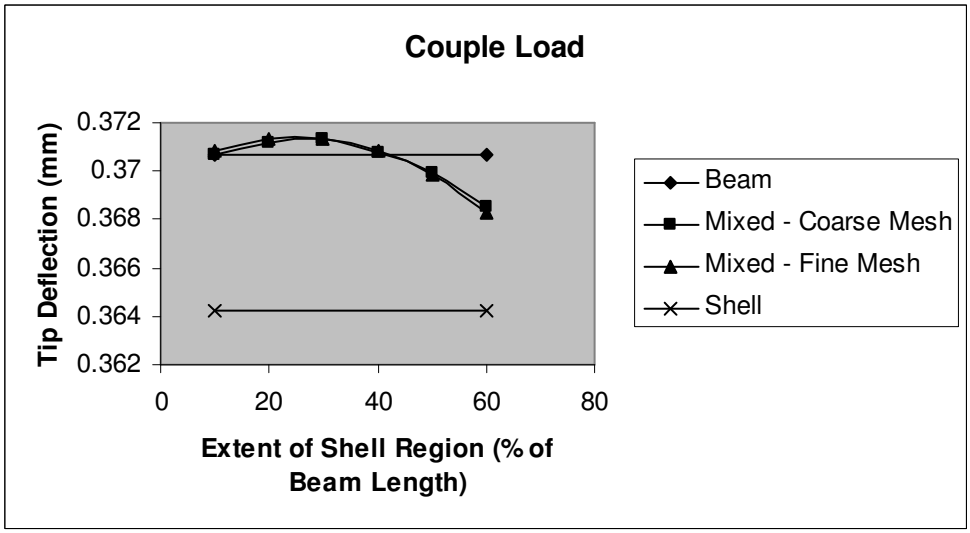

Fig. 6-10 Tip Deflection vs. Extent of Shell Region for Couple Load

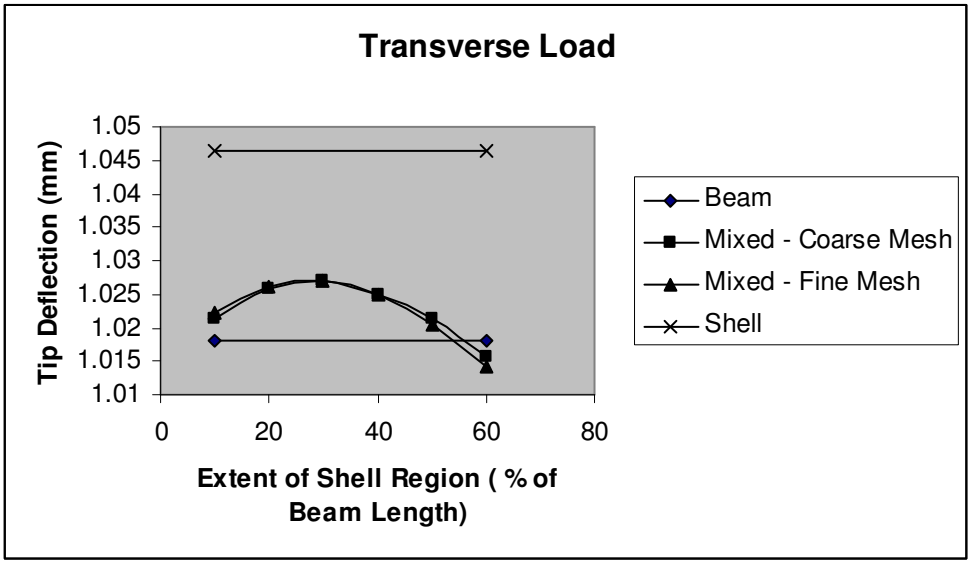

Fig. 6-11 Tip Deflection vs. Extent of Shell Region for Transverse Load

Comparisons and Comments

It can be seen that the mixed model provides acceptably good results of tip deflection for axial, couple and transverse loading cases. For example, the percent errors between the full shell model and mixed model with 30% shell region are 0.6% for axial load, 2% for couple and transverse loads. For axial load and couple loads, the mixed model results approach the full shell results as the extent of shell region increases. For transverse load, mixed model results approach the full shell model result in the beginning and then start to

move away. This is most probably due to the approximate nature of the shear stress distribution assumed in the derivation of the constraint equations.

6.2.2 Cantilever with RBS

The cantilever of Example 1 is considered with RBS next (Fig. 6-12). The RBS data is as given below. The RBS dimensions are taken within the limitations given by FEMA 350 [4].

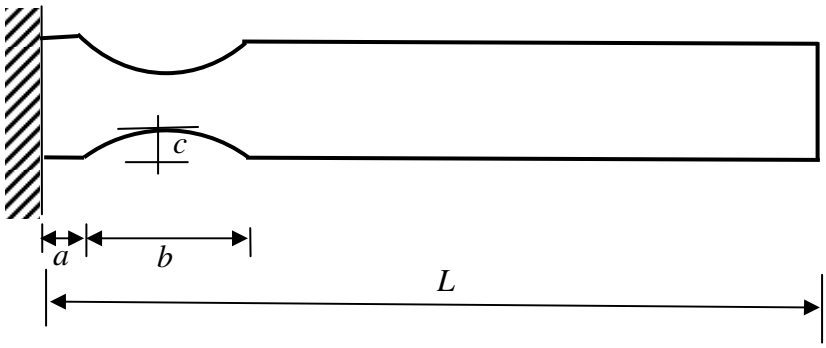

RBS Data:

a = 200 mm
b = 350 mm
c = 70 mm

L = 4 m

Fig. 6-12 Cantilever Beam with RBS

Full Shell Model

The full shell model of the beam with RBS consisting of 212 shell elements is shown in Fig. 6-13 below.

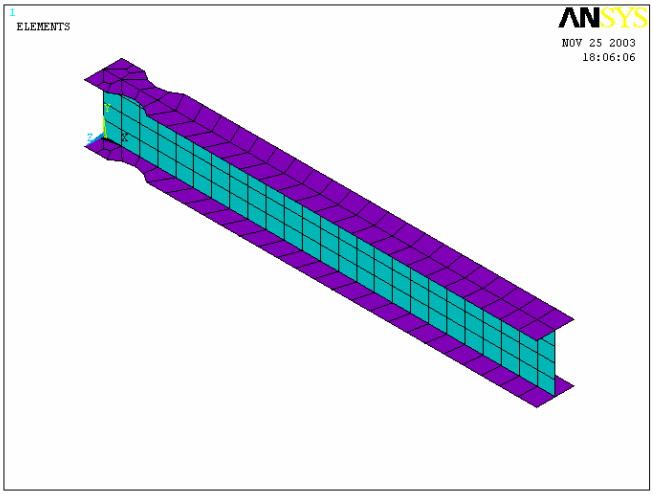

Fig. 6-13 Full Shell Model of Cantilever Beam with RBS

Mixed Model

The cantilever beam with RBS is modeled as a mixed dimensional model of beam and shell elements. Coupling has again been achieved using the constraint equations derived in Chapter 5. Various lengths of shell regions have been considered. An example of a mixed model in which the shell region extends over 30% of beam length (this corresponds to 76 shell elements) is shown in Fig. 6-14.

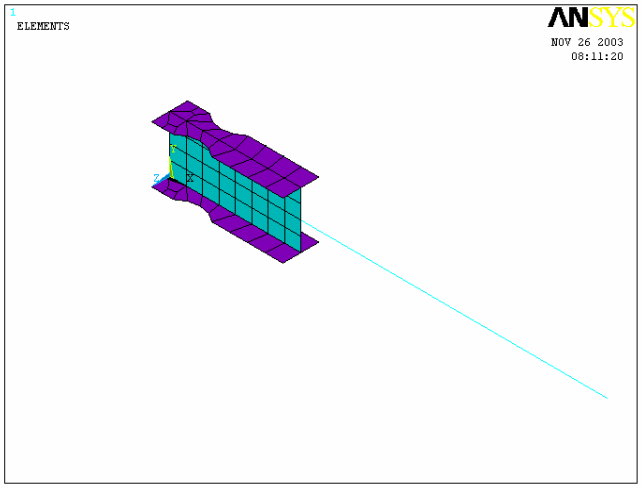

Fig. 6-14 Mixed Model of Cantilever with RBS

Axial Load

The axial normal stress distribution as a result of a 10 kN axial tensile force is shown in Fig. 6-15.

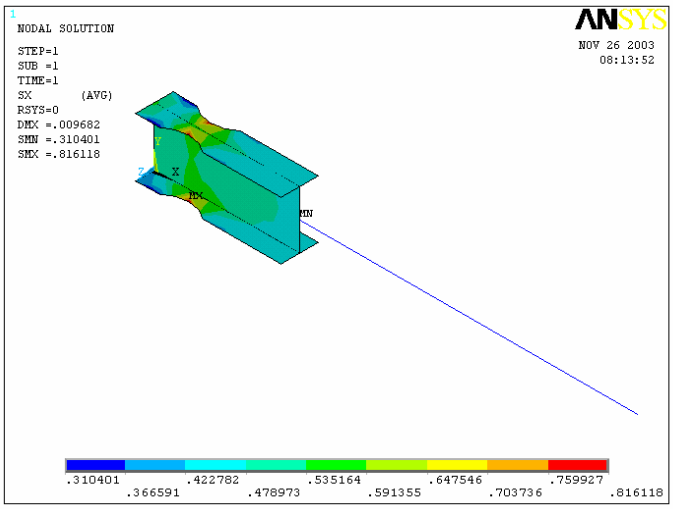

Fig. 6-15 Normal Stress Distribution of Cantilever with RBS under Axial Load

Couple Load

The mixed model of the cantilever with RBS is subjected to an end couple of 10 kN-m. The resulting normal stress distribution is shown in Fig. 6-16 below.

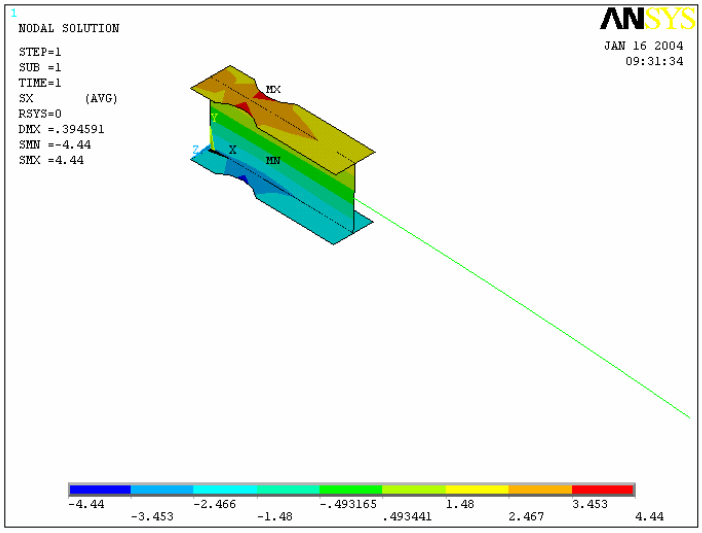

Fig. 6-16 Normal Stress Distribution of Cantilever Beam with RBS under Couple Load

Transverse Load

The mixed model is subjected to a 10 kN force applied vertically downward at the free end with the resulting normal stress and shear stress distribution as shown in Fig. 6-17 and Fig. 6-18.

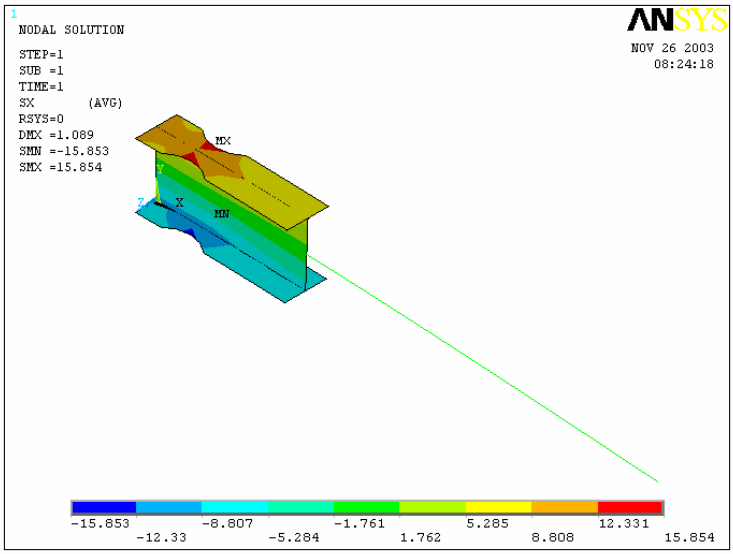

Fig. 6-17 Normal Stress Distribution of Cantilever Beam with RBS under Vertical Load

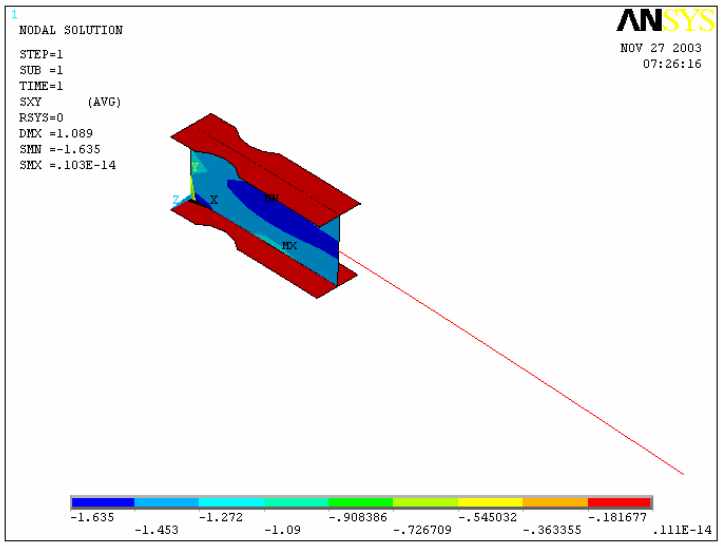

Fig. 6-18 Shear Stress Distribution of Cantilever with RBS under Vertical Load

From the contour plots of the normal stress distributions under axial, couple and transverse loads, it can be seen that there is no stress disturbance at the mixed dimensional interface which is an indication valid coupling has been achieved for axial force, bending moment and shear force.

Summary of Results

A summary of the results of full shell and mixed models of cantilever with RBS under axial load and transverse load has been given in Table 6-6. The axial and transverse tip deflections are the quantities of interest.

Table 6-6: Summary of Results - Cantilever with RBS

Model	Shell Region (% of Beam Length)	Axial Tip Deflection (mm) (due to axial load of 10kN)	Transverse Tip Deflection (mm) (due to couple load of 10kN.m)	Transverse Tip Deflection (mm) (due to transverse load of 10kN)
Mixed	20	0.0097019	0.39527	1.1123
Mixed	30	0.0096817	0.39459	1.1099
Mixed	40	0.0096716	0.39442	1.1090
Mixed	50	0.0096548	0.39285	1.1027
Shell	100	0.00962220	0.38719	1.1289

Comparisons and Comments

It is again noted that the mixed dimensional models give acceptably accurate results for the tip deflection under axial, couple and transverse loading. The percent error between the full shell model and the mixed model with 30% shell region are 0.6% for axial load and 2% for couple and transverse loads. Especially in the presence of RBS, in which theoretical analysis cannot be easily applied, the mixed models provide an accurate model of the problem. Like in the case of beam without RBS, for axial and couple loadings the results of the mixed models approach that of the full shell model as the percentage of the shell region is increased. For transverse loading, the mixed model results deviate from the full shell model as the shell region is increased. The reasons for this might be, as mentioned above, the approximate nature of the shear stress distribution employed in deriving the constraint equations and also local effects of load application in the full shell model. Nevertheless, the mixed models provide a rational, efficient and sufficiently accurate method of analysis in the presence of RBS.

Increase in Deflection due to the Presence of RBS

The percent increases in tip deflection due to the presence of RBS can be computed from the full shell and mixed models for axial and transverse loading as follows.

Axial Load

From the full shell model: Percent Increase = 2.5 %

From mixed model with 30 % shell region: Percent Increase = 2.4 %

Couple Load

From the full shell model: Percent Increase = 6.3 %

From mixed model with 30 % shell region: Percent Increase = 8.3 %

Transverse Load

From the full shell model: Percent Increase = 7.9 %

From mixed model with 30% shell region: Percent Increase = 7.0 %

Thus it can be seen that the percent increases in deflections due to the presence of RBS obtained from the full shell model and mixed model with 30% shell region are very close.

6.2.3 Cantilever Beam with Maximum Cut RBS

To study the effects of maximum cut allowable by FEMA 350 [4], the cantilever beam of Example is considered with the maximum cut. The RBS dimensions corresponding to the maximum cut as given by FEMA 350 are:

$$a = 0.5b_f = 165\,\text{mm}$$
$$b = 0.85h = 453\,\text{mm}$$
$$c = 0.25b_f = 82.5\,\text{mm}$$

The beam with maximum cut is subjected to a 10 kN force applied axially and vertically downward. Full shell model and mixed models (with variable lengths of shell regions) have been considered. Table 6-7 and gives a summary of the results obtained.

Table 6-7: Summary of Results of Cantilever Beam with Maximum RBS Cut

Model	Shell Region (% of Beam Length)	Axial Tip Deflection (mm) (due to axial load of 10kN)	Transverse Tip Deflection (mm) (due to couple load of 10kN.m)	Transverse Tip Deflection (mm) (due to transverse load of 10kN)
Mixed	20	0.0098391	0.40867	1.1600
Mixed	30	0.0098137	0.40778	1.1571
Mixed	40	0.0098031	0.40738	1.1548
Mixed	50	0.0097896	0.40630	1.1499
Shell	100	0.0097528	0.39986	1.1741

Increase in Deflections due to Maximum Cut RBS

Axial Load

From full shell model: Percent Increase = 4.0 %

From mixed model with 30% shell region: Percent Increase = 4.0 %

Couple Load

From full shell model: Percent Increase = 9.8 %

From mixed model with 30 % shell region: Percent Increase = 12.0 %

Transverse Load

From full shell model: Percent Increase = 12.2 %

From mixed model with 30% shell region: Percent Increase = 12.7 %

It is seen that the full shell and mixed model with 30% shell region give very similar results for percent increase in tip deflections for axial and transverse loading. We also see that the percent increase in tip deflection under transverse load exceeds the maximum percent increase of 9% provided by FEMA 350 [4].

6.3 EXAMPLE 2: INVERTED L-FRAME

The second example considered is the inverted L-frame shown in Fig. 6-19. Full shell model and mixed model of the problem has been presented.

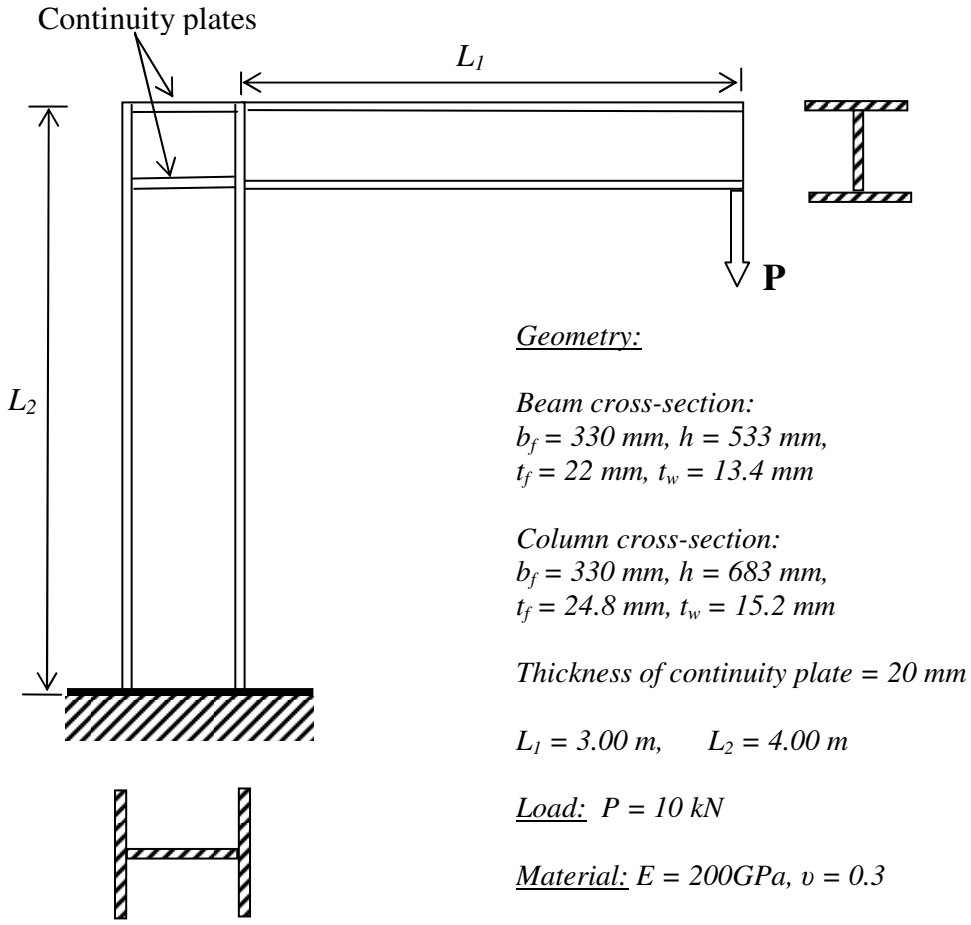

Fig. 6-19 Example 2: Inverted L-Frame

6.3.1 Inverted-L Frame without RBS

Full Shell Model

The frame is initially modeled as a full shell model as shown in Fig. 6-20.

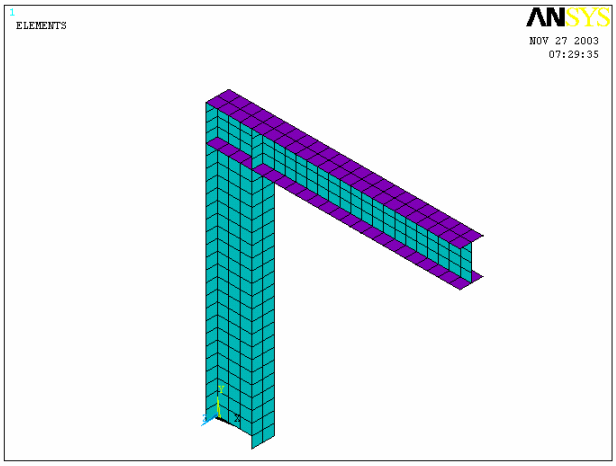

Fig. 6-20 Full Shell Model of Inverted-L Frame without RBS

Mixed Model

The frame is also modeled as a mixed beam-shell. Like the case of the cantilever beam, the length of the shell region has been varied. The shell region in the beam and column has been taken as some percentage of the beam and column lengths, respectively (Fig.6-21).

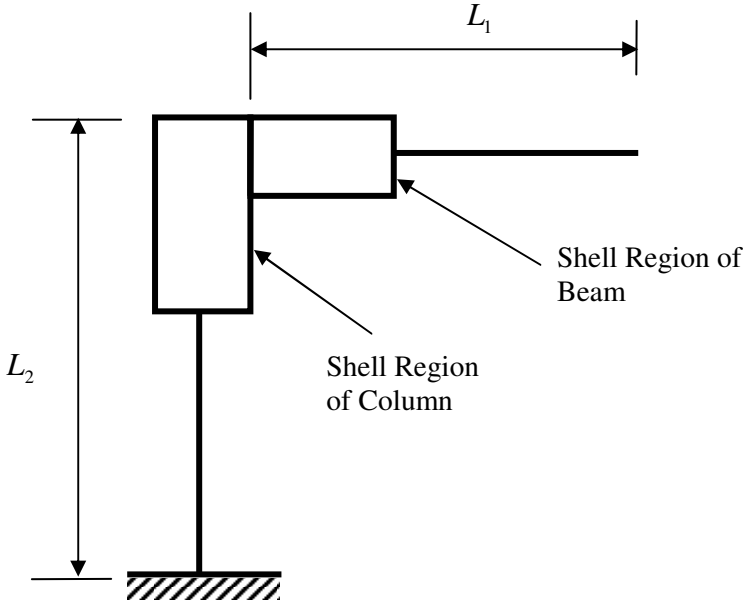

Fig. 6-21 Extent of Shell Regions in Beam and Column

A mixed model of the frame in which the shell regions in the beam and column extend over 30 % of the beam and column lengths is shown in Fig. 6-22.

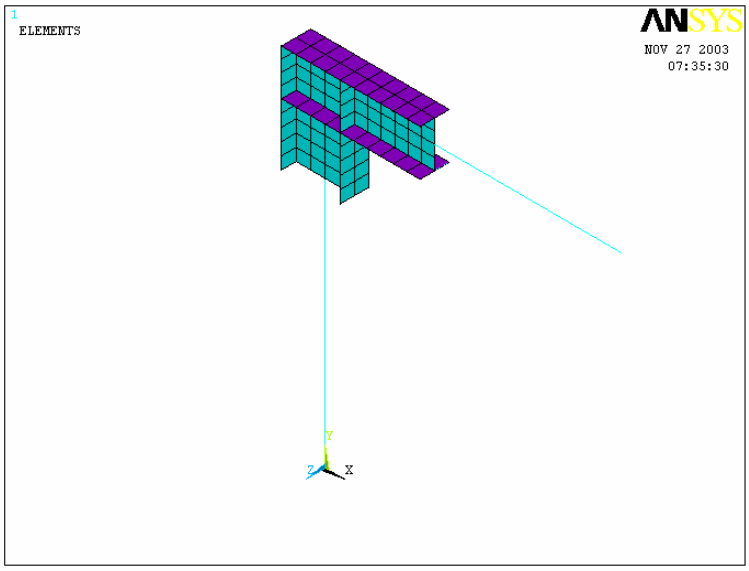

Fig. 6-22 Mixed Model of Inverted-L Frame without RBS

The distribution of normal stress and shear stress is indicated in Fig. 6-23 and Fig. 6-24. It can again be seen that there is no stress disturbance in the mixed dimensional interface and the constraint equations provide valid coupling between beam and shell elements.

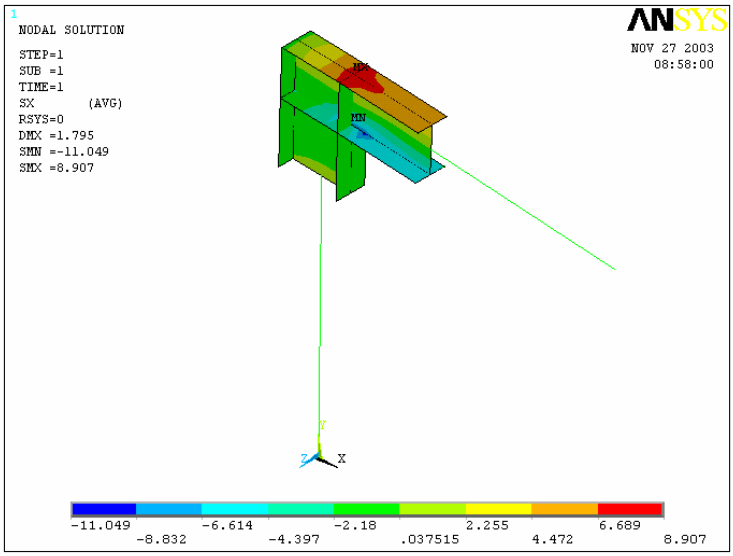

Fig. 6-23 Normal Stress Distribution of Inverted-L Frame

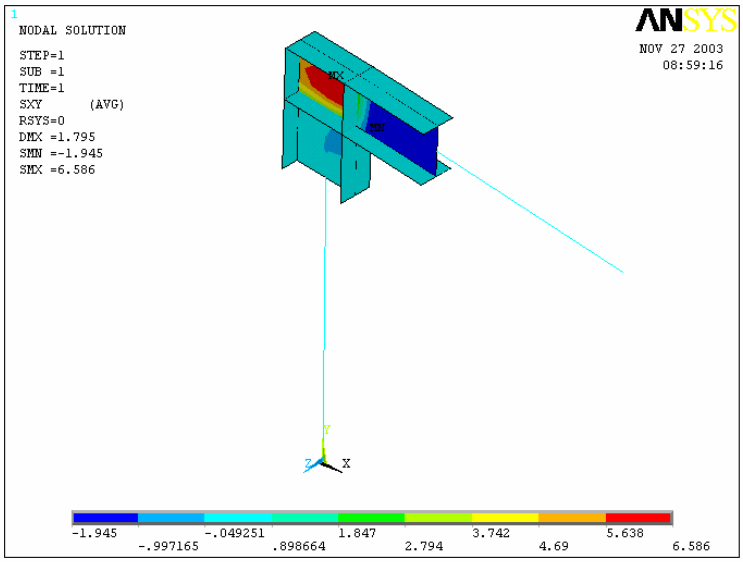

Fig. 6-24 Shear Stress Distribution of Inverted-L Frame

Results from Elementary Beam Theory

The tip deflections are computed based on elementary beam theory. The results are presented below. The frame model of the problem is shown in Fig.6-25. Centerline dimensions have been taken and rigid beam-column joint has been assumed.

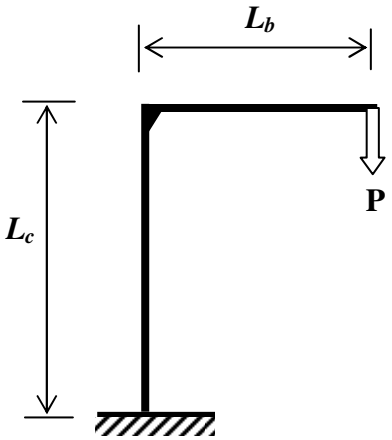

P = 10 kN

Beam:
$L_b = 2658.5\ mm$
$A_b = 21073\ mm^2$
$I_b = 1079026892\ mm^4$

Column:
$L_c = 3733.5\ mm$
$A_c = 25996\ mm^2$
$I_c = 2095486653\ mm^4$

Material: E = 200 GPa

Fig. 6-25 Frame Model of Inverted-L Frame

The tip displacements in the horizontal and vertical directions computed using elementary mechanics of materials are as follows.

Vertical Deflection

Vertical deflection due to flexural deformations:

$$\Delta_{flexure} = \frac{PL_b^2 L_c}{EI_c} + \frac{PL_b^3}{3EI_b} + \frac{PL_c}{A_c E} = 0.92701\,\text{mm} \quad \text{... (6-6)}$$

Vertical deflection due to shear deformations:

$$\Delta_{shear} = \frac{PL_b}{A_s G} = 0.01975\,\text{mm} \quad \text{... (6-7)}$$

Thus total vertical deflection is:

$$\Delta_{total} = 0.94676\,\text{mm}$$

Horizontal Deflection

$$\Delta_h = \frac{PL_b L_c}{2EI_c} = 0.44210\,\text{mm} \quad \text{... (6-8)}$$

Summary of Results

The tip deflection of the inverted frame has been considered for comparison of the full shell and mixed models of the frame as shown in Table 6-8.

Table 6-8: Summary of Results - Inverted-L Frame without RBS

Model	Shell Region (% of Beam Length)	Axial Tip Deflection (mm)	Transverse Tip Deflection (mm)
Beam	0	0.44210	0.9468
Mixed	20	0.69781	1.7818
Mixed	30	0.70274	1.7005
Mixed	40	0.70262	1.7076
Mixed	50	0.70237	1.6870
Shell	100	0.72131	1.9340

Comparisons and Comments

It is seen that the results of the full shell and mixed models are close to each other. The difference between the full shell model and mixed model results can be explained by the fact that there are local effects at load application in the full shell model and that the constraint equations were derived by assuming an approximate shear stress distribution in accordance with simple beam theory. On the other hand, results from theory of elementary mechanics of materials are significantly different from those of full shell or mixed models. In fact, the deflections obtained by simple beam theory with rigid beam-column joint assumption are much smaller than those obtained by full shell or mixed models. The main reason is most probably the fact that the given beam-column detail does not satisfy the rigid joint assumption. Additional reinforcement of the joint is needed to approach the rigid beam-column assumption. The mixed and full shell models, however, give more realistic models by taking into account the actual deformations within the joint. The mixed model, in which only the connection area is modeled by shell, provides an efficient and sufficiently accurate representation of the problem.

6.3.2 Inverted-L Frame with RBS

The frame is now considered with the previous RBS data which is repeated below:

RBS Data:

a = 200 mm
b = 350 mm
c = 70 mm

The frame with the above RBS data is modeled as a full shell as well as mixed beam-shell models. The extents of the shell region in the beam and column have been varied as in the case of frame without RBS.

Full Shell Model

The full shell model of the inverted-L frame with RBS is shown in Fig. 6-26 below.

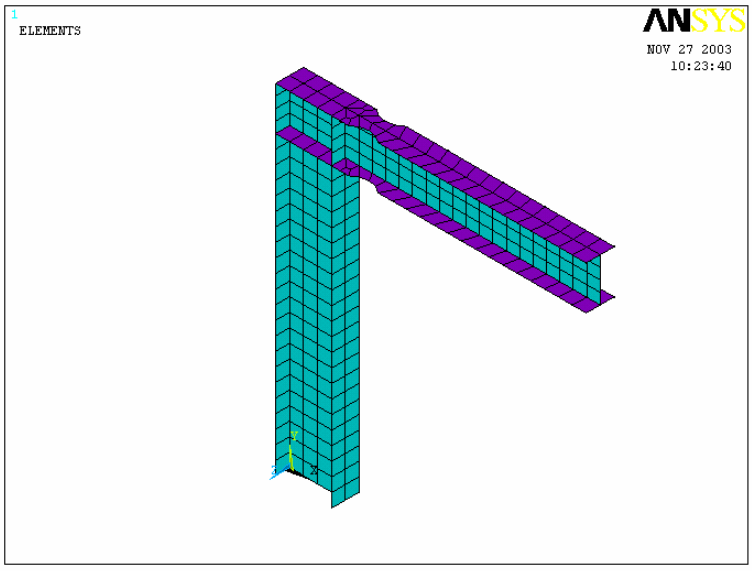

Fig. 6-26 Full Shell Model of Inverted-L Frame with RBS

Mixed Model

A mixed model of the inverted frame with RBS in which the shell regions in the beam and column extend over 30 % of the beam and column lengths respectively is shown in Fig. 6-27.

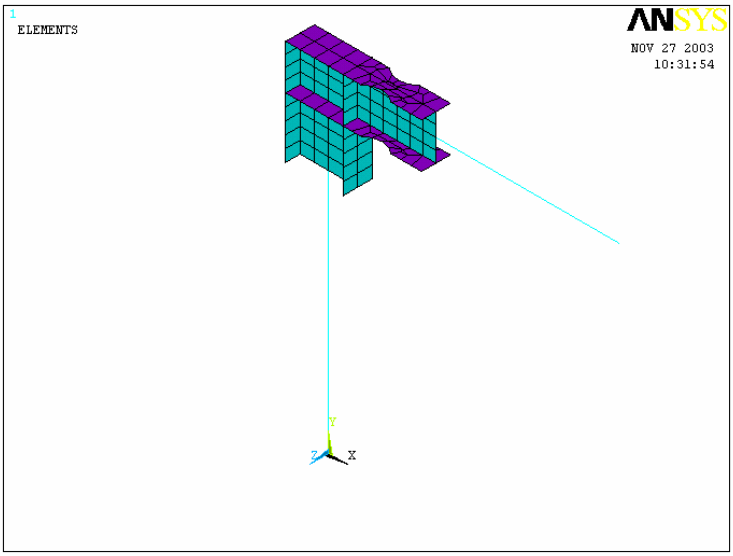

Fig. 6-27 Mixed Model of Inverted-L Frame with RBS

The distributions of normal stresses in the x-direction and shear stresses in the xy plane are shown in Fig. 6-28 and Fig. 6-29.

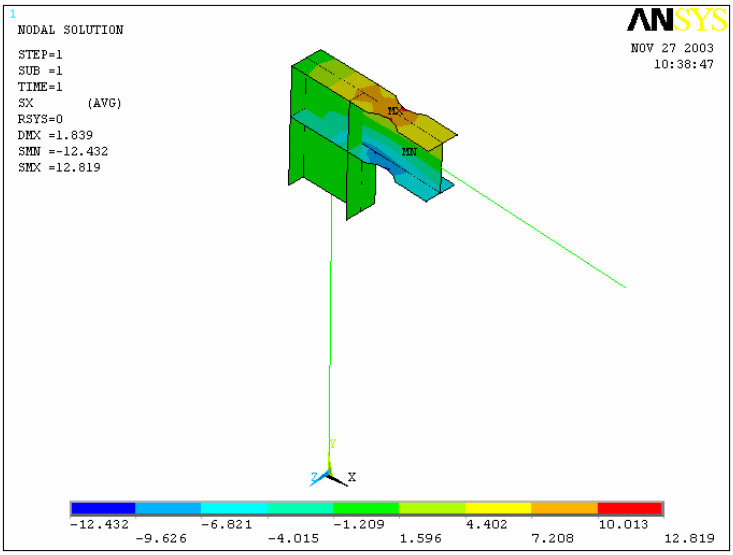

Fig. 6-28 Normal Stress Distribution of Inverted-L Frame with RBS

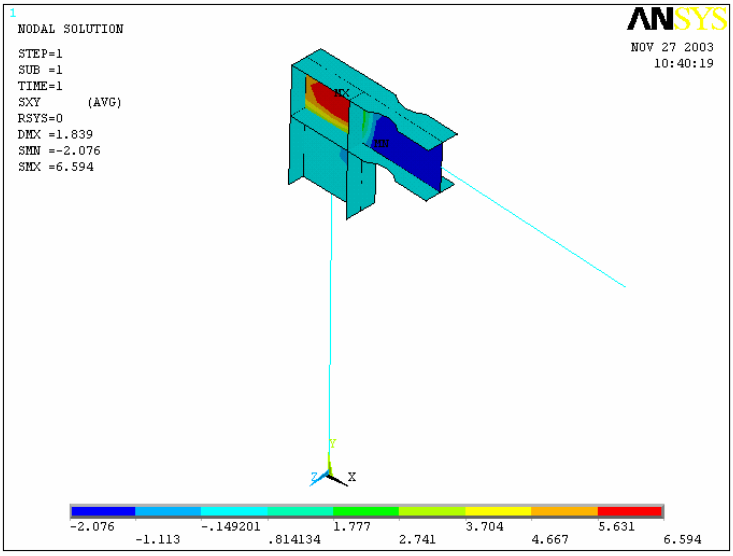

Fig. 6-29 Shear Stress Distribution of Inverted-L Frame with RBS

Summary of Results

The summary of results of inverted-L frame with RBS is shown in Table 6-9.

Table 6-9. Summary of Results - Inverted-L Frame with RBS

Model	Shell Region (% of Beam Length)	Horizontal Tip Deflection (mm)	Vertical Tip Deflection (mm)
Mixed	20	0.70371	1.7775
Mixed	30	0.70719	1.7623
Mixed	40	0.70682	1.7505
Mixed	50	0.70655	1.7406
Shell	100	0.72552	1.9800

Increase in Deflection due to the Presence of RBS

From full shell model: Percent Increase = 2.4 %

From mixed model with 30% shell region: Percent Increase = 3.6 %

6.3.3 Inverted-L Frame with Maximum Cut

Maximum cut as allowed by FEMA 350 [4] is applied to the inverted-L frame. The dimensions of the maximum allowable RBS cut are given in Sec. 6.2.3 and are repeated below.

$a = 0.5b_f = 165\,\text{mm}$

$b = 0.85h = 453\,\text{mm}$

$c = 0.25b_f = 82.5\,\text{mm}$

The frame with maximum cut is modeled as a full shell model and mixed models (with variable regions of shell regions). A summary of the results of tip displacements obtained is given in Table 6-9.

Summary of Results

The results obtained are summarized in Table 6-10 below.

Table 6-10. Summary of Results - Inverted-L Frame with Maximum Cut RBS

Model	Shell Region (% of Beam Length)	Horizontal Tip Deflection (mm)	Vertical Tip Deflection (mm)
Mixed	30	0.70955	1.7813
Mixed	40	0.70926	1.7753
Mixed	50	0.70909	1.7662
Shell	100	0.72807	2.0056

Increase in Deflection due to Maximum Cut RBS

From full shell model: Percent Increase = 3.7 %

From mixed model with 30% shell region: Percent Increase = 4.8 %

Comparisons and Comments

We again observe that the mixed model provides an efficient and sufficiently accurate model of the inverted L-frame with RBS connection. In the presence of RBS, in which simple beam theory cannot be applied, the mixed model provides a rational, sufficiently accurate and efficient analysis method of moment frames with RBS.

Chapter 7
Conclusions and Further Work

7.1 CONCLUSIONS

An efficient and accurate analysis method for the analysis of moment frames with RBS has been presented. The method relies on the development of multi-point constraint equations by equating the work done on either side of a mixed dimensional interface. The resulting stress distribution is in agreement with that given by elastic theory.

A basic requirement for the development of the constraint equations is the determination of stress distribution at the mixed dimensional interface. Stress distributions due to axial force and bending moment are given quite accurately using simple beam theory. The stress distribution due to shear force based on thin-wall theories is found to give acceptably good results.

Constraint equations are developed for shell-beam transition of an arbitrary I-section for axial load, bending moment and shear force for a four node isoparametric shell element. A Fortran 90 code has been written to develop constraint equations from cross-section and mesh data. The developed constraint equations have been implemented using the finite element program ANSYS. The resulting stress distributions do not exhibit stress disturbance at the mixed dimensional interface. The results are also in close agreement with full shell models of the problems considered.

It has been shown that mixed dimensional modeling using multi-point constraint equations provides an accurate and efficient method for the elastic analysis of moment frames with RBS. The mixed dimensional model provides a more realistic representation of the joint area. Unlike the frame model in which joints are commonly assumed to be rigid, the mixed dimensional model considers deformations within the connection. The

mixed dimensional analysis is more rational and accurate than the current provision of simply increasing the drift by a certain percentage.

It has been shown that frame model with rigid joints may significantly underestimate deflections unless the joint has been properly detailed so as to validate the rigid-joint assumption. The mixed model, on the other hand, considers the actual deformations in the joint region, and thus yields more realistic deflections corresponding to a given joint detail.

7.2 FURTHER WORK

In the present study it has been shown that mixed dimensional analysis using multi-point constraint equations provides an efficient and accurate analysis of moment frames with RBS. However, the work is not exhaustive and there are a number of avenues for improvement and further investigation such as those given below.

1. The mixed dimensional models were implemented in rather simple examples due the limitation of the available ANSYS version. Although these examples are sufficient to show the validity of the developed constraint equations, it would have been preferable to consider more realistic frame models. Implementation of the constraint equations in larger frame models can be undertaken with a better version of ANSYS or other FE software that can incorporate constraint equations.

2. Multi-point constraint equations are dependent on the element type. In this study constraint equations are derived for a four node quadrilateral shell element. Constraint equations for other types of shell elements can be developed using the same approach. In particular constraint equations for an eight or nine node shell element, which can model curved edges more accurately, can be derived. In addition, moment frames can be represented as solid-beam mixed model in which case it is necessary to derive constraint equations for the transition between solid and beam elements.

3. The length over which the shell region extends from the connection is an important one which should be answered in such a way as to balance accuracy and computation. It depends on a number of factors such as connection detail, RBS data, beam and column dimensions, and type of loading among others. Further study to systematically arrive at an optimum length of shell region is necessary.

4. A program for the analysis moment frames with RBS using multi-point constraint equations approach can be taken up as an area of further work. The program is to input frame geometry including RBS data and loading and output displacements and stresses. Meshing of joint area, development and incorporation of constraint equations is to be handled internally by the program.

Appendix A

Beam-Shell Coupling Program

A.1 BASIC ASSUMPTIONS

The wide flange I-section is meshed using *four node isoparametric shell elements* whose shape functions are given by $N_i = 1/4(1 \pm \xi)(1 \pm \eta)$ such as the SHELL63 ANSYS element.

A.2 INPUT DATA

The input data to the program consists of two sets of data:

Line 1: beam cross sectional data
h (height), b (width), tf (flange thickness), tw (web thickness)

Line 2: mesh data
nf (# of subdivisions of flange), nw (# of subdivisions of web)

NB: The flange and the web are each divided into a number of equal segments. The # of subdivisions of flange must be an even number.

A.3 PROGRAM OUTPUT

The program generates five linear homogeneous shell-beam constraint equations for a wide flange I-section corresponding to the following actions:

1. Axial force: *Fz*
2. Bending about the *x*-axis: *Mx*
3. Bending about y-axis: *My*
4. Shear force in direction *y*: *Fy*
5. Shear force direction *x*: *Fx*

For each constraint equation coefficients of the relevant degree of freedom are given by the program. The constant term of each of the constraint equations is zero. That is each constraint equation can be expressed as: $\sum coeff \times DOF = 0$

The constraint equations are given with respect to a *local xyz coordinate system*. Also the shell nodes having the equal magnitudes of coefficients are classified into four categories for convenience in output generation. The user will have to interpret the results with respect to the global coordinate system and actual shell node numbers.

A.4 LOCAL COORDINATE SYSTEM

The constraint equations are given with respect to local coordinate system shown in Fig. A-1. The axial direction is the local z-direction; the x-axis is the major principal axis; the *y*-axis is the minor principal axis.

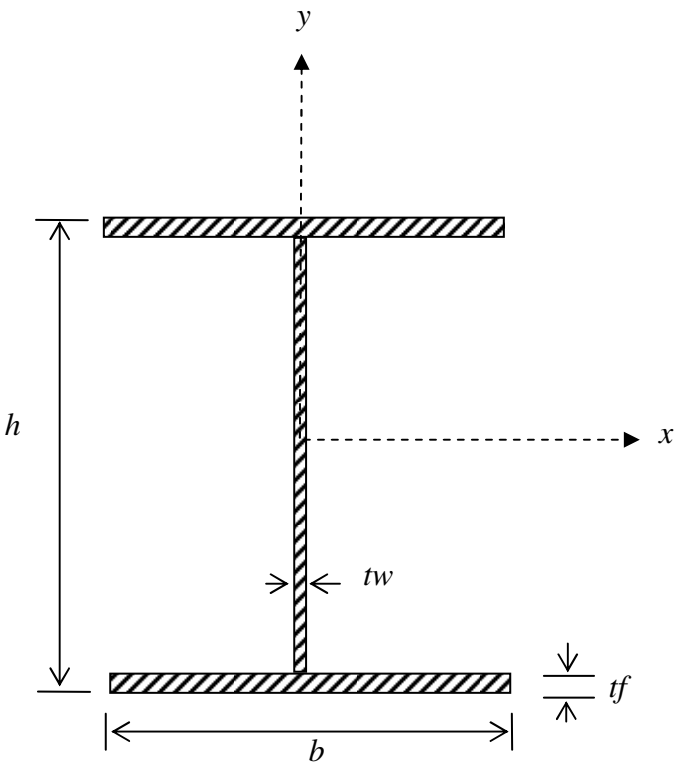

Fig. A-1 Local Coordinate System of I Section

A.5 SHELL NODE NOMENCLATURE

The shell nodes are grouped into four categories for concise output.

1. Flange edge nodes (always present)
2. Flange interior nodes (present if $nf \geq 4$)
3. Corner nodes (always present)
4. Web nodes (present if $nw \geq 2$)

An example of the shell node category scheme is illustrated in Fig. A-2 below. The program gives the absolute values of the coefficients of the shell node DOF, and the user should interpret the results correctly. For axial and shear forces, the coefficients of all shell node DOF are positive. For bending, the coefficients of the shell node translations on one side of the neutral axis are positive and those on the other side are negative.

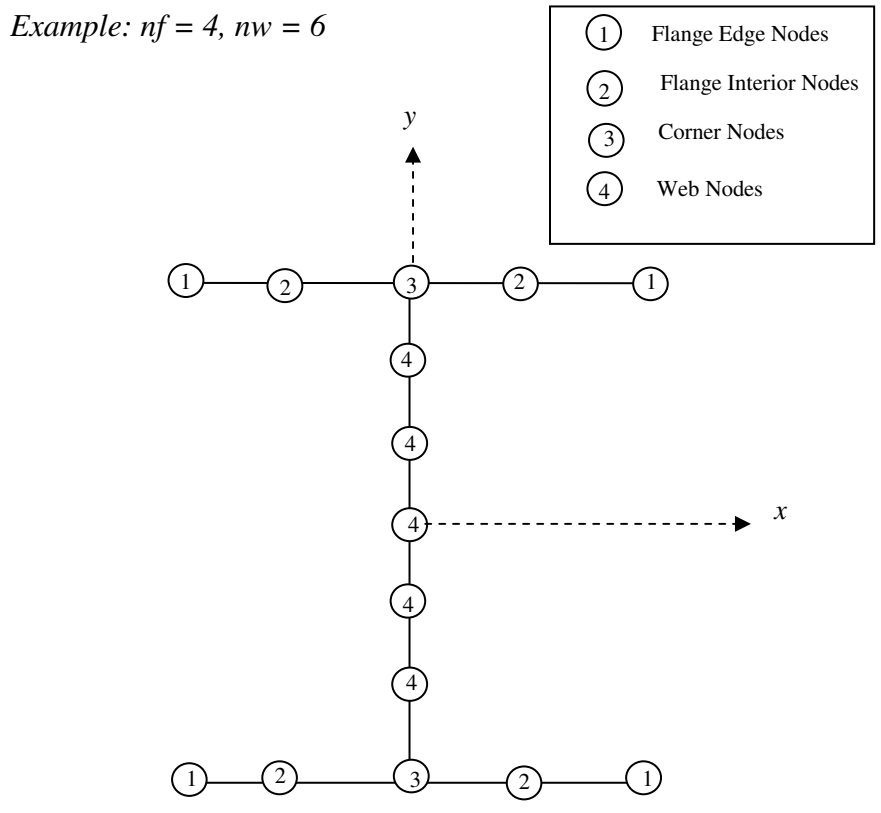

Fig. A-2 Shell Node Nomenclature

A.6 PROGRAM LISTING

```
Program CONSTRAINT
!-----------------------------------------------------------------------------------------------
! Computes Beam-Shell Constraint Equations of an I-section. The I section is meshed
! into four node isoparametric shell elements. The flange and the web are divided into
! elements of equal edge length.
!
! Input:
!       Beam cross section data:
!          H = height
!          b = width
!          tf = thickness of flange
!          tw = thickness of web
!
!       Mesh data:
!            nf = # of elements in flange
!            nw = # of elements in web
! Output:
!        5 Constraint equations
!      (1 for Axial: Fz, 2 for Bending: Mx, Mx, 2 for Shear: Fx, Fy )
!
! Written by: Dawit Hailu, AAU (August 2003)
!
!-----------------------------------------------------------------------------------------------
implicit none
integer:: nf, nw, i
real*8  h, b, tf, tw, hf, A, hw, Ixx, Iyy, c1, c2, c3, c4, c5, c6, c7, k, x, y, delx, dely
real*8  m1, m2, m3, m4, m5, m6
open (10, file = 'const.in', status = 'old', action = 'read')
open (11, file = 'const.out', status = 'replace', action = 'write')
! read cross-sectional constants
read (10,*) h , b , tf , tw
! read mesh constants
read (10,*) nf , nw
if ( nf /= 2* (nf/2) ) then
    write (11,*) 'ERROR 01: The # of elements in flange (nf) must be even ! '
    stop
end if
hf = h - tf
delx = b / nf
dely = hf / nw
! ------------------------------ axial coupling ------------------------------------------
A = 2 * tf * b + tw * hf
```

```
c1 = tf * delx/2.
c2 = tw * dely/2.
write                                                                                    (11,*)
'*************************************************************************
*******'
write (11,*) '*                                                          *'
write (11,*) '*   The program generates beam-shell constraint equations for a wide flange
*'
write (11,*) '*   I-section.                                               *'
write (11,*) '*                                                          *'
write (11,*) '*   Written by: Dawit Hailu, AAU, Addis Ababa. (August 2003)          *'
WRITE (11,*) '*                                                          *'
write (11,*) '*                                                          *'
write(11,*)  '************************************************************'
write (11,*)
! input echo
write (11,*) '                          Input Echo                       '
write (11,*) '-------------------------------------------------------------------------'
write (11,*)
write (11,*) 'Height = ',h
write (11,*) 'Width = ',b
write (11,*) 'Flange thickness =',tf
write (11,*) 'Web thickness =',tw
write (11,*) 'No. of divisions of flange =',nf
write (11,*) 'No. of divisions of web =',nw
write (11,*)
write (11,*) '                          Program Output                   '
write (11,*) '-------------------------------------------------------------------------'
write (11,*) '                          Axial Coupling                   '
write (11,*) '-------------------------------------------------------------------------'
write (11,*)
write (11,*) ' Coefficient of beam node           = ', -A, 'uz'
write (11,*) ' Coefficient of flange edge nodes   = ', c1, 'uz'
if ( nf >= 4 ) then
  write (11,*) ' Cofficient of flange interior nodes = ', 2*c1, 'uz'
end if
write (11,*) ' Cofficient of corner nodes         = ', 2*c1 + c2, 'uz'
if ( nw >= 2 ) then
  write (11,*) ' Coefficient of web nodes           = ', 2*c2, 'uz'
end if
!------------------------------ bending coupling ----------------------------------------
! a) Bending about the x-axis
hw = h - 2.*tf
Ixx = ( b * h**3 -b * hw**3 + tw * hw**3 ) / 12.
c3 = hf * tf * delx / 4.
c4 = tf**3 * delx / 24.
```

```
write (11,*)
write (11,*) '-------------------------------------------------------------------------------'
write (11,*) '                    Bending Coupling -- About x-axis                           '
write (11,*) '-------------------------------------------------------------------------------'
write (11,*)
write (11,*) ' Coefficient of beam node                  = ', -Ixx, 'rotx'
write (11,*) ' Coefficient of flange edge nodes            = ', c4, 'rotx'
if ( nf >= 4 ) then
  write (11,*) ' Coefficient of flange interior nodes        = ', 2.*c4, 'rotx'
end if
write (11,*) ' Coefficient of corner nodes               = ', 2.*c4, 'rotx'
write (11,*) ' Coefficient of flange edge nodes            = ', c3, 'uz'
if ( nf >= 4 ) then
  write (11,*) ' Coefficient of flange interior nodes        = ', 2*c3, 'uz'
end if
! compute coeffcicients of web and corner nodes translations
if ( nw == 1 ) then
     k = hf / 6.
     c5 = k * c2
     write (11,*) ' Coefficient of corner nodes               = ', 2.*c3 + c5, 'uz'
elseif ( nw == 2 ) then
     k = hf / 3.
     c5 = k * c2
     write (11,*) ' Coefficient of corner nodes               = ', 2.*c3 + c5, 'uz'
elseif ( nw == 2 * ( nw / 2 ) ) then
      y = dely
      do i = 1, ( nw/2 -1 )
        k = 2.* y
        c5 = k * c2
        write (11,*) ' Coefficient of ',i,'th web nodes         = ', c5, 'uz'
        y = y + dely
      end do
      k = hf/2. - dely/3.
      c5 = k * c2
      write (11,*) ' Coefficient of corner nodes               = ', 2.*c3 + c5, 'uz'
else
      y = dely/2.
      do i = 1, ( nw - 1 )/2
         k = 2.* y
         c5 = k * c2
         write (11,*) ' Coefficient of ',i,'th web nodes      =', c5, 'uz'
         y = y + dely
      end do
      k = hf/2. - dely/3.
      c5 = k * c2
      write (11,*) ' Coefficient of corner nodes               = ', 2.*c3 + c5, 'uz'
```

```
end if
! b) Bending about the y-axis
Iyy = ( 2.* tf * b**3 + hw * tw**3 ) /12.
c6 = tw**3 * dely/24.
write (11,*)
write (11,*) '-------------------------------------------------------------------------------'
write (11,*) '                    Bending Coupling -- About y axis                    '
write (11,*) '-------------------------------------------------------------------------------'
write (11,*) ' Coefficient of beam node  = ', -Iyy, 'roty'
write (11,*) ' Coefficient of web nodes  = ', 2.*c6, 'roty'
write (11,*) ' Coeffient of corner nodes = ', c6, 'roty'
! compute coefficients of flange nodes
if ( nf == 2 ) then
  k = b/3.
  c5 = k * c1
  write (11,*) ' Coefficient of flange edge nodes = ', c5, 'uz'
else
  x = delx
  do i = 1, ( nf/2 - 1 )
    k = 2. * x
    c5 = k * c1
    write (11,*) 'Coefficient of', i,'th flange interior nodes = ', c5,'uz'
    x = x + delx
  end do
  k = b/2. - delx/3.
  c5 = k * c1
  write (11,*) ' Coefficient of flange edge nodes = ', c5, 'uz'
endif

! ------------------------ shear coupling ---------------------------------
! a) In the y-direction
write (11,*)
write (11,*) '-------------------------------------------------------------------------------'
write (11,*) '                    Shear Coupling -- Direction y                    '
write (11,*) '-------------------------------------------------------------------------------'
write (11,*) ' Coefficient of beam node =', -Ixx, 'uy'
m1 = b*( h**2 - hw**2 ) / (16.*tf)
m2 = ( h**2 - hw**2 ) / (8.*tf)
m3 = ( b * h**2 - b * hw**2 + tw * hw**2 ) / (8.*tw)
m4 = 0.5
!    Coefficients of web nodes
if ( nw == 1 ) then
   k = hf**2 /24.
   c7 = c2 * ( m3 - k*m4 )
   write (11,*) ' Coefficient of corner nodes = ',c7, 'uy'
elseif ( nw == 2 * (nw/2) ) then
```

```
    y = 0
    do i = 1, nw/2
      k = 3.* y**2 + (2./3.)* dely**2
      c7 = c2 * ( 2.*m3 - k*m4 )
      write (11,*) ' Coefficient of',i,'th web nodes = ',c7, 'uy'
      y = y + dely
    end do
    k = (3./8.)* hf**2 - (2./3.)* hf * dely + (1./3.)* dely**2
    c7 = c2 * ( m3 - k*m4 )
    write (11,*) ' Coefficient of corner nodes  = ',c7, 'uy'
else
    y = dely/2
    do i = 1, (nw-1)/2
      k = 3.* y**2 + (2./3.)* dely**2
      c7 = c2 * ( 2.* m3 - k*m4 )
      write (11,*) ' Coefficient of',i,'th web nodes = ',c7, 'uy'
      y = y + dely
    end do
    k = (3./8.)* hf**2 - (2./3.)* hf * dely + (1./3.)* dely**2
    c7 = c2 * ( m3 - k*m4 )
    write (11,*) ' Coefficient of corner nodes  = ',c7, 'uy'
endif
! Coefficient of flange nodes
if ( nf == 2 ) then
     k = b/3.
     c7 = c1 * ( m1 - k*m2 )
     write (11,*) ' Coefficient of flange edge nodes = ', c7, 'ux'
else
    x = delx
    do i = 1, (nf/2 -1)
      k = 2.*x
      c7 = c1 * ( 2.*m1 - k*m2 )
      write (11,*) ' Coefficient of',i,'th flange interior node = ',c7, 'ux'
      x  = x + delx
    end do
    k = b/2. - delx/3.
    c7 = c1 * ( m1 - k*m2 )
    write (11,*) ' Coefficient of flange edge nodes =',c7, 'ux'
endif
! b) In the x-direction
m5 = b**2 /4.
m6 = 0.5
write (11,*)
write (11,*) '-------------------------------------------------------------------------------'
write (11,*) '                        Shear Coupling -- Direction x                          '
write (11,*) '-------------------------------------------------------------------------------'
```

```
write (11,*) ' Coefficient of beam node = ', -Iyy, 'ux'
x = 0.
do i = 1, nf/2
   k = 3. * x**2 + (2./3.) * delx**2
   c7 = c1 * ( 2.* m5 - k*m6)
   if ( i == 1 ) then
      write (11,*) ' Coefficient of corner nodes = ',c7, 'ux'
   else
      write (11,*) ' Coefficient of',i-1,'th flange interior node = ', c7,'ux'
   endif
   x = x + delx
end do
k = (3./8.)* b**2 - (2./3.)* b * delx + (1./3.)* delx**2
c7 = c1 * ( m5 - k*m6)
write (11,*) ' Coefficient of flange edge nodes  = ', c7,'ux'
end program  CONSTRAINT
```

Appendix B
SHELL63 ELEMENT

B.1 ELEMENT DESCRIPTION

SHELL63 has both bending and membrane capabilities. Both in-plane and normal loads are permitted. The element has six degrees of freedom at each node: translations in the nodal x, y, and z directions and rotations about the nodal x, y, and z-axes. Stress stiffening and large deflection capabilities are included. A consistent tangent stiffness matrix option is available for use in large deflection (finite rotation) analyses.

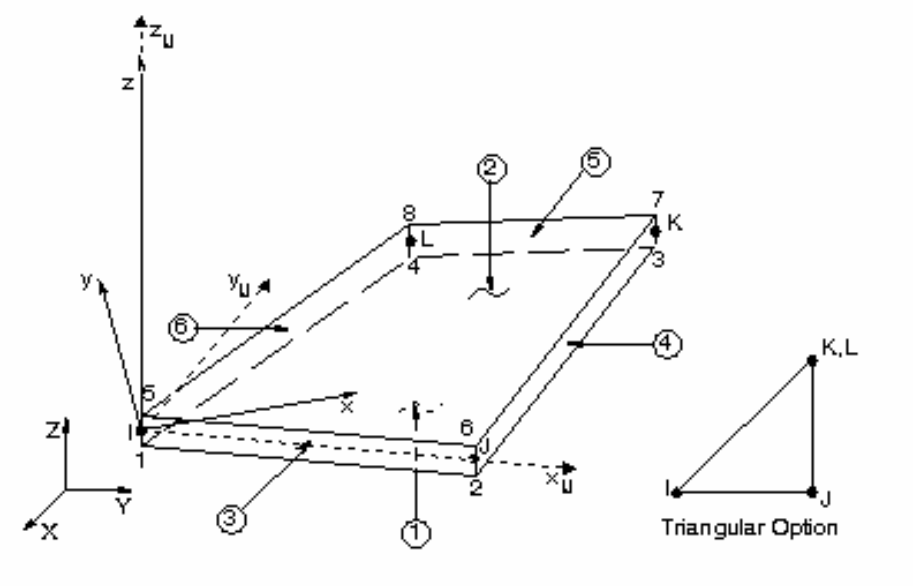

Fig. B-1. SHELL63 Elastic Shell Element

B.2 INPUT DATA

The geometry, node locations, and the coordinate system for this element are shown in Fig. B-1. The element is defined by four nodes, four thicknesses, an elastic foundation stiffness, and the orthotropic material properties. Orthotropic material directions correspond to the element coordinate directions. The element x-axis may be rotated by an angle THETA (in degrees).

The thickness is assumed to vary smoothly over the area of the element, with the thickness input at the four nodes. If the element has a constant thickness, only TK(I) need be input. If the thickness is not constant, all four thicknesses must be input.

Pressures may be input as surface loads on the element faces as shown by the circled numbers on Fig.B-1. Positive pressures act into the element. Edge pressures are input as force per unit length. The lateral pressure loading may be an equivalent (lumped) element load applied at the nodes or distributed over the face of the element. The equivalent element load produces more accurate stress results with flat elements representing a curved surface or elements supported on an elastic foundation since certain fictitious bending stresses are eliminated.

Temperatures may be input as element body loads at the "corner" locations (1-8) shown in Fig. B-1. The first corner temperature T1 defaults to TUNIF. If all other temperatures are unspecified, they default to T1. If only T1 and T2 are input, T1 is used for T1, T2, T3, and T4, while T2 (as input) is used for T5, T6, T7, and T8. For any other input pattern, unspecified temperatures default to TUNIF.

SHELL63 Input Summary

Element Name

SHELL63

Nodes

I, J, K, L

Degrees of Freedom

UX, UY, UZ, ROTX, ROTY, ROTZ

Real Constants

TK(I), TK(J), TK(K), TK(L), EFS, THETA,

RMI, CTOP, CBOT, (Blank), (Blank), (Blank),

(Blank), (Blank), (Blank), (Blank), (Blank), (Blank),

ADMSUA

Material Properties

EX, EY, EZ, (PRXY, PRYZ, PRXZ or NUXY, NUYZ, NUXZ),

ALPX, ALPY, ALPZ, DENS, GXY, DAMP

Surface Loads

Pressures --

face 1 (I-J-K-L) (bottom, in +Z direction),

face 2 (I-J-K-L) (top, in -Z direction),

face 3 (J-I), face 4 (K-J), face 5 (L-K), face 6 (I-L)

Body Loads

Temperatures --

T1, T2, T3, T4, T5, T6, T7, T8

Special Features

Stress stiffening, Large deflection, Birth and death

KEYOPT(1)

0 --

Bending and membrane stiffness

1 --

Membrane stiffness only

2 --

Bending stiffness only

B.3 OUTPUT DATA

The solution output associated with the element is in two forms:

- nodal displacements included in the overall nodal solution
- additional element output as shown in Element Output Definitions

Printout includes the moments about the x face (MX), the moments about the y face (MY), and the twisting moment (MXY). The moments are calculated per unit length in the element coordinate system. The element stress directions are parallel to the element coordinate system.

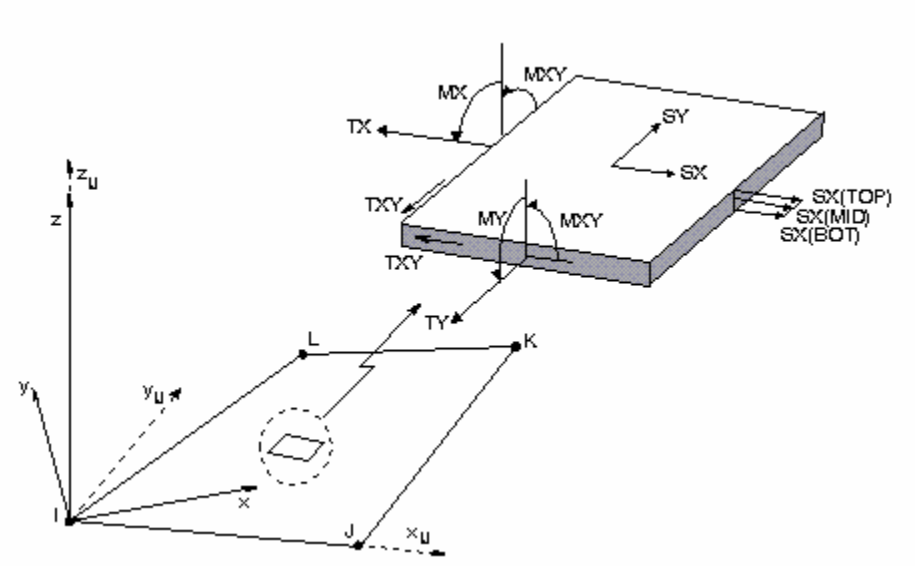

Fig. B-2 SHELL63 Stress Output

Appendix C

Effective Shear Area of I-Section

The effective shear area can be given as:

$$A_s = A / f_s \qquad \text{... (C-1)}$$

where f_s is cross-sectional constant known as the form factor and given by:

$$f_s = \frac{A}{I^2} \int_A \frac{Q^2}{t^2} dA \qquad \text{... (C-2)}$$

where A = cross-sectional area, I = moment of inertia of cross-section, Q = first moment of area above a given level about the neutral axis, t = the width of the cross-section at a given level.

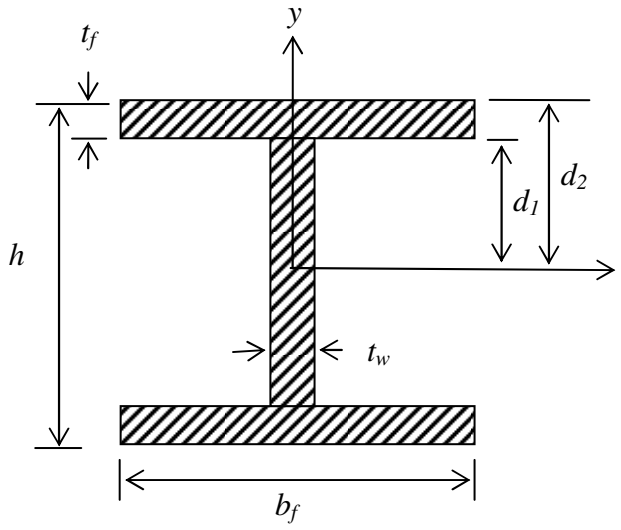

Fig. III-1 Cross-sectional Parameters of an I-Section

For the I-section shown in Fig. III-1, the form factor for shear is given by:

$$f_s = f_{sf} + f_{sw} = \frac{2A}{I^2}\int_{d_1}^{d_2}\frac{Q_f^2}{b_f}dy + \frac{2A}{I^2}\int_{0}^{d_1}\frac{Q_w^2}{t_w}dy \qquad \text{... (C-3)}$$

where f_{sf} and f_{sw} are the contributions of the flange and web respectively.

The first moments of area corresponding to the flange and web are given by:

$$Q_f = \int_{y}^{d_2} y b_f dy = \frac{b_f}{2}\left(d_2^2 - y^2\right) \qquad y \geq d_1 \qquad \text{...(C-4)}$$

$$Q_w = \int_{d_1}^{d_2} y t_f dy + \int_{y}^{d_1} y t_w dy = \frac{b_f}{2}\left(d_2^2 - d_1^2\right) + \frac{t_w}{2}\left(d_1^2 - y^2\right) \qquad 0 \leq y \leq d_1$$

After inserting the above expressions in Eq. (III-3) and simplifying, one obtains the following expression for the form factor:

$$f_s = \frac{\frac{9}{2}\left\{\frac{1}{\alpha}(1-\beta)+\beta\right\}\left\{\frac{1}{\alpha^2}\left[\frac{\beta^5}{2}-\beta^3+\frac{\beta}{2}\right]+\frac{1}{\alpha}\left[-\frac{23}{30}\beta^5+\beta^3-\frac{\beta}{2}+\frac{8}{30}\right]+\frac{8}{30}\beta^5\right\}}{\left[\frac{1}{\alpha}\left(1-\beta^3\right)+\beta^3\right]^2}$$

...(C-5)

where

$$\alpha = \frac{t_w}{b_f} \qquad \text{and} \qquad \beta = \frac{d_1}{d_2} = \frac{h - t_f}{h}.$$

References

1. Davis, G., "Steel Moment-frame Buildings: The Saga Continues", Part I, *Structural Engineer*, April 2001.

2. Davis, G., "Steel Moment-frame Buildings: The Saga Continues", Part II, *Structural Engineer*, June 2001.

3. Federal Emergency Management Agency (FEMA), "FEMA 353: Recommended Specifications and Quality Assurance Guidelines for Steel Moment-Frame Construction for Seismic Applications", FEMA, June 2001.

4. Federal Emergency Management Agency (FEMA), "FEMA 350: Recommended Seismic Design Criteria for New Steel Moment-Frame Buildings", FEMA, June 2001.

5. Engelhardt, M. D., Winneberger, T., Z., A. J., Potyraj, T. J., "The Dogebone Connection: Part II", *Modern Steel Construction*, August 1995.

6. Great Lakes Fabricators and Erectors Association, http://www.glfea.org/html/id-dogbones.htm, TIME

7. Kinde, S.K., "A New FEA-based Stiffness Matrix Exact Modeling of RBS Members in Special Moment Resisting Frames using FEA Building Analysis Programs", personal correspondence, June 2003.

8. Hinton, E., Owen, D.R.J., "Finite Element Programming", Academic Press, London, 1989.

9. Cook, R. D., Malkus, D. S., Plesha, M.E., "Concepts and Applications of Finite Element Analysis", John Wiley & Sons, New York, 1989.

10. Cook, R. D., "Finite Element Modeling for Stress Analysis", John Wiley & Sons, New York, 1995.

11. Monaghan, D. J., "Automatically Coupling Elements of Dissimilar Dimension in Finite Element Analysis", Ph.D. Dissertation, Queens University of Belfast, Sept. 2000.

12. Craig, R. R., "Mechanics of Materials", John Wiley & Sons, New York, 1996.

13. ANSYS Release 6.1, ANSYS Inc., 1994.